Simulation of gallium nitride vertical fin-shaped field effect transistor for use as thermal neutron detector

by

Bryce L. Davidson

B.S., Fort Hays State University, 2020

A THESIS

submitted in partial fulfillment of the
requirements for the degree

MASTER OF SCIENCE

Alan Levin Department of Mechanical and Nuclear Engineering
Carl R. Ice College of Engineering

KANSAS STATE UNIVERSITY
Manhattan, Kansas

2023

Approved by:

Major Professor

NSC-614-5769 11/2023

Unclassified Unlimited Release

Copyright

© Bryce L. Davidson 2023.

NSC-614-5769 11/2023

Unclassified Unlimited Release

Abstract

Through the use of a radiation detection system simulation framework, a gallium nitride vertical fin-shaped field effect transistor (FinFET) was studied for output response when utilized as a thermal neutron detector. The FinFET was assumed to had been backfilled with boron carbide, reactive to thermal neutrons. The GaN FinFET was modeled with radiation transport from MCNP, and the electronic transport from COMSOL Multiphysics. Fabricated FinFET devices (not neutron reactive) were tested to aid in the tuning of the COMSOL FinFET model. Through time-depenent studies, the drain current response pulse to simulated ionization due to single events lead to building of a database of device responses to radiation. By integrating the current pulses over time, the induced charge was calculated. Using the results of the radiation transport PTRAC file in combination with the induced charge database, an integrated charge spectrum was calculated.

NSC-614-5769 11/2023

Unclassified Unlimited Release

Table of Contents

List of Figures . . . viii

List of Tables . . . xii

Acknowledgements . . . xiii

1 Introduction . . . 1

1.1 Motivation . . . 1

1.2 Simulation Framework . . . 4

1.3 Hardware . . . 6

2 Radiation Transport Simulation . . . 10

2.1 Model . . . 10

3 Fabricated FinFET Device Testing . . . 13

4 Electronic Transport Simulation . . . 17

4.1 COMSOL FinFET Model . . . 17

4.2 Meshing Techniques . . . 20

4.3 Particle Ionization Simulation . . . 21

5 Results . . . 27

5.1 Radiation Transport Results . . . 27

5.2 Fabricated FinFET Device Tesing Results . . . 31

5.3 Electronic Transport Results . . . 32

5.4 Combined Radiation and Electronic Transport Results . . . 37

NSC-614-5769 11/2023

Unclassified Unlimited Release

6 Conclusions 47
6.1 Future Work 49
Bibliography 51

NSC-614-5769 11/2023
Unclassified Unlimited Release

List of Figures

1.1 Illustration of FinFET device geometry[1]. 4

1.2 Flowchart of simulation framework used to analyze radiation detection systems. 5

1.3 Kyma Technologies sample FinFET devices under probe station microscope. 7

1.4 Cross-section image of fabricated GaN FinFETs, with material annotations[2]. 8

1.5 Reaction products from neutron-boron capture reaction[3]. 9

2.1 Illustration of FinFET model and thermal neutron source placement. Not to scale. 11

2.2 Illustration of half of FinFET model materials and dimensions. Not to scale. 12

3.1 Illustration of wiring schematic for Kansas State testing of FinFET devices[2]. 15

3.2 Kansas State probe station, with dark box enclosure and microscope, including the Keithley 237 High Voltage Source and computer for measurement collection. 16

4.1 COMSOL model of 2D GaN vertical FinFET. This model includes the charge generation domain (small domain located in the fin) with gate dielectric material and conducting semiconductor material in order to use metal gate contact physics. 18

4.2 The meshing used for time-dependent solutions, zoomed out (left) and focused on the generation domain (right). In order to converge on a solution in COMSOL, the meshing must match the physics. 21

4.3 Bragg curve for 1777 keV alpha particle traveling through GaN, calculated from SRIM/TRIM. 22

NSC-614-5769 11/2023

Unclassified Unlimited Release

4.4 Cumulative Bragg curve for 1777 keV alpha particle traveling through GaN, calculated from SRIM/TRIM and numerically calculated using Python. . . . 25

5.1 Histogram of energy values of alpha particles incident on GaN. 28
5.2 Histogram of energy values of lithium ions incident on GaN. 28
5.3 Histogram of location values of incident alpha particles along the fin edge. Arc length of 0 µm corresponds to bottom (drain) of the device and arc length of 3.5 µm corresponds to the top (source) of the device. 29
5.4 Histogram of location values of incident alpha particles along the base of the trench. Arc length of 0 µm corresponds to bottom (drain) of the device and arc length of 3.5 µm corresponds to the top (source) of the device. 29
5.5 Histogram of location values of incident lithium ions along the fin edge. Arc length of 0 µm corresponds to bottom (drain) of the device and arc length of 3.5 µm corresponds to the top (source) of the device. 30
5.6 Histogram of location values of incident lithium ions along the base of the trench. Arc length of 0 µm corresponds to bottom (drain) of the device and arc length of 3.5 µm corresponds to the top (source) of the device. 30
5.7 Comparison of fabricated GaN FinFET S1D5 measured family of curves, Kyma Technologies and KSU. 31
5.8 Comparison of fabricated GaN FinFET S3F6 measured family of curves, Kyma Technologies and KSU. 32
5.9 Comparison of fabricated GaN FinFET S4D5 measured family of curves, Kyma Technologies and KSU. 32
5.10 By keeping the gate bias constant and sweeping the drain bias, a family of curves is simulated in COMSOL. 34
5.11 By changing the static electron mobility in the COMSOL simulation model, the current-voltage curve (black) can be adjusted to match measured devices (red). Gate bias of 3 V. 35

NSC-614-5769 11/2023
Unclassified Unlimited Release

5.12 COMSOL stationary results showing the the electron concentration, hole concentration, and electric potential for the off state GaN FinFET. 36
5.13 Comparison of y-component of electric field down center cutline of GaN FinFET simulation for gate bias of −0.3 V and −5 V, with a constant drain bias of 5 V. Arc length of 0 µm corresponds to bottom (drain) of the device and arc length of 3.5 µm corresponds to the top (source) of the device. 37
5.14 Location of where incident particles are simulated in COMSOL. Note the angles given are referenced according the perpendicular of the side of the fin edge. 38
5.15 Time-dependent solution snapshots of 900 keV alpha particle ionization simulated. Snapshot times: 1.95 ns, 2.0025 ns, 2.067 ns, 2.126 ns, 4 ns, 8.5 ns. . . 39
5.16 Output drain current from simulated 900 keV alpha particle ionization, see Fig. 5.15, full pulse (left) and zoomed in of peak (red outline). 40
5.17 Angular interpolated integrated charge values for 50 keV and 800 keV alpha particle COMSOL simulations. 41
5.18 Angular interpolated integrated charge values for 50 keV and 800 keV lithium ion COMSOL simulations. 42
5.19 Integrated charge spectrum including alpha particles and lithium ions. The value of N represents the number of times the particles were incident on the GaN surface– the total number of source thermal neutrons simulated was 5,517,789. 43
5.20 Integrated charge spectrum including only alpha particles. The value of N represents the number of times the particles were incident on the GaN surface– the total number of source thermal neutrons simulated was 5,517,789. 43
5.21 Integrated charge spectrum including only lithium ions. The value of N represents the number of times the particles were incident on the GaN surface– the total number of source thermal neutrons simulated was 5,517,789. 44

NSC-614-5769 11/2023
Unclassified Unlimited Release

5.22 Integrated charge spectrum including only alpha particles incident on fin edge. The value of N represents the number of times the particles were incident on the GaN surface– the total number of source thermal neutrons simulated was 5,517,789. 44

5.23 Integrated charge spectrum including only alpha particles incident on base of trench. The value of N represents the number of times the particles were incident on the GaN surface– the total number of source thermal neutrons simulated was 5,517,789. 45

5.24 Integrated charge spectrum including only lithium ions incident on fin edge. The value of N represents the number of times the particles were incident on the GaN surface– the total number of source thermal neutrons simulated was 5,517,789. 45

5.25 Integrated charge spectrum including only lithium ions incident on base of trench. The value of N represents the number of times the particles were incident on the GaN surface– the total number of source thermal neutrons simulated was 5,517,789. 46

6.1 By increasing the drift length (changing how far away the drain contact is to the fin) and maintaining the same geometric doping length in COMSOL, the on-resistance of the GaN FinFET can be tuned. 50

NSC-614-5769 11/2023

Unclassified Unlimited Release

List of Tables

1.1 Properties of silicon and gallium nitride. 2

3.1 Equipment and materials used in the FinFET hardware testing. 13

NSC-614-5769 11/2023

Unclassified Unlimited Release

Acknowledgments

This work was funded by the Department of Energy's Kansas City National Security Campus, operated by Honeywell Federal Manufacturing & Technologies, LLC under contract number DE-NA0002839.

Part of the computing for this project was performed on the Beocat Research Cluster at Kansas State University, which is funded in part by NSF grants CNS-1006860, EPS-1006860, EPS-0919443, ACI-1440548, CHE-1726332, and NIH P20GM113109.

NSC-614-5769 11/2023

Unclassified Unlimited Release

Chapter 1

Introduction

1.1 Motivation

The control and shortage of ^{3}He gas creates a demand for alternative neutron detectors. Solid-state detectors offer rigidity to mechanical damage and typically require lower voltage to operate as compared to gas detectors. Due to the neutral charge of the neutron, methods to detection are indirect– meaning detectors observe secondary products due to neutron interactions with matter. Neutron detectors have been developed using neutron conversion layers, which takes advantage of neutron capture reactions, where an incident neutron is absorbed by a nucleus and the unstable isotope then quickly emits ions or gamma rays. Through material activation, a material could also absorb a neutron and create an isotope that then later decays into ionizing radiation and be detected.

Semiconductors are used for radiation detection in part because of their unique property to either conduct or insulate due to a gap in the electronic valence and conduction bands, called the band gap. Ionizing radiation can promote electrons from the valence band to the conduction band, which allows an electric current to pass through the device. When used in combination with a solid-state conversion material, either through an alloying process or through a thin film applied on the material of the detector, the reaction products may be detected. Typically, semiconductor detectors like Si(Li) or HPGe are used for x-ray or

NSC-614-5769 11/2023

Unclassified Unlimited Release

gamma-ray detection, and require cool temperatures to mitigate electronic background noise. Semiconductors like HgI_2 and CdZnTe are also used for x-ray and gamma-ray detection, but they also have intrinsic thermal neutron detection capabilities due to prompt gamma products from neutron capture in Hg and Cd[4;5]. Wide band gap materials like gallium nitride and silicon carbide have grown in popularity due to their electronic and thermal properties, with recent studies starting to investigate it capabilities for transistors in harsh radiation environments.

Gallium nitride (GaN) is a wide band gap semiconductor material that has properties relevant to ionizing radiation detection. Some of these properties include its thermal conductivity, electron mobility, and composition of low atomic number elements with high threshold displacement damage values. Properties of GaN and their values are compared to silicon in Table 1.1[6;7].

Table 1.1: *Properties of silicon and gallium nitride.*

	Si	**GaN**
Density [$g\,cm^{-3}$]	2.33	6.15
Band Gap [eV]	1.12	3.39
Average Ionization Energy [eV]	3.61	8.9-10
Thermal Conductivity [$W\,cm^{-2}\,K^{-1}$]	1.5	1.3
Mobility Electrons [$cm^2\,V^{-1}\,s^{-1}$]	1450	1000
Mobility Holes [$cm^2\,V^{-1}\,s^{-1}$]	450	30
Critical Electric Field [$MV\,cm^{-1}$]	0.3	3.3
Displacement Energy [eV]	13	18 (Ga), 22 (N)

Gallium nitride has also been shown to be sensitive to alpha particles and low energy x rays, while not very sensitive to high-energy gamma rays and x rays[8–10]. The material has shown intrinsic sensitivity to neutron radiation, mostly from the ^{14}N(n,p) reaction with a neutron capture cross sectional area of 79.5 ± 1.4 mb[11], and has been studied for use as a neutron scintillation detector[12]. Although there is intrinsic neutron sensitivity in GaN, using a neutron conversion layer, like ^{6}LiF, was shown to increase collection efficiency by two orders of magnitude as compared to bare Si-doped GaN[12]. These characteristics of GaN provide a solid-state option for neutron detection with gamma discrimination via calibration.

Another benefit of GaN for ionizing radiation detection purposes comes from its radiation hardness qualities, which allows the material to withstand harsh radiation environments like

NSC-614-5769 11/2023
Unclassified Unlimited Release

nuclear reactors or space. This is due of the strength of nitrogen-gallium bonds, tested through radiation degradation experiments[13–16] using protons, neutrons, and gamma rays. Material defect studies using ion beams and molecular dynamic studies have shown that GaN typically accumulates point defects, causing traps and higher recombination probability, which often can be annealed[17;18].

When it comes to solid-state thermal neutron detectors, charge collection is key, and the geometry of the device impacts both where ionization is likely to occur and where the active detection region is located. Planar PIN diodes utilize a thin film conversion layer on top of the device, limiting the solid angle of reaction products to the detector's active region, but have an active detection region near the conversion layer. Microstructured neutron detectors (MSND) are designed to incorporate a PIN diode's active region and include deep trenches into the diode that can be backfilled with the neutron conversion layer, increasing thermal neutron detection efficiency[19]. A trenched device geometry has potential to be a thermal neutron radiation detector if it has an active detection region near the conversion material, low background device current, and scalability. The device geometry addressed in this thesis is the GaN vertical fin-shaped field effect transister (FinFET).

The GaN FinFET has a raised "fin" from the bulk of the GaN, which separates the source and drain contacts, shown in Fig. 1.1, and requires only n-type doped GaN. The FinFET also features two dielectrically insulated gate contacts along both sides of the fin walls, controlling the flow of current through the device. The FinFET geometry has some adaptability in the width and height of the fin as well as the length the gate can travel up the sides of the fin. The device has two main operating states, the on-state and off-state. The on-state implies that current is allowed to flow through the device while the off-state shunts the current flow. When operating the FinFET, bias on the drain and gate contacts are with respect to the source contact, such that the drain bias V_D is the same as V_{DS} and the gate bias V_G is the same as V_{GS}. It is customary that the source contact V_S is grounded and the drain bias is greater than 0 V, and that a gate bias that is greater than 0 V is the on-state while a gate bias that is less than or equal to 0 V is the off-state. The GaN FinFET can be manufactured as a single fin device or multifin device (up to 60 fins), according Kyma

NSC-614-5769 11/2023
Unclassified Unlimited Release

Technologies, Inc.

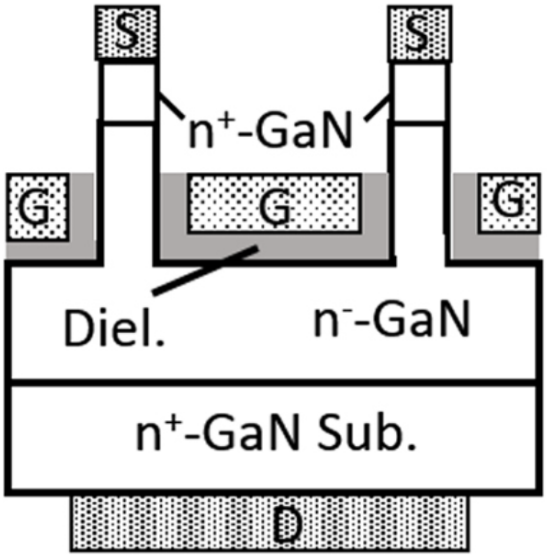

Figure 1.1: *Illustration of FinFET device geometry*[1].

1.2 Simulation Framework

To see if the GaN FinFET would work as an effective thermal neutron detector, a simulation framework was utilized that incorporated radiation transport and electronic charge transport, based off of previous work[20;21]. The framework includes radiation transport codes of MCNP6.2 and SRIM/TRIM[22]. To simulate the electronic charge transport in the GaN FinFET, COMSOL Multiphysics[23] was used. If necessary, electronic circuit simulation to the device can be simulated using LTspice. The framework is set up such that any device geometry may be simulated and analyzed, utilizing a workflow as shown in Fig. 1.2.

MCNP, a Monte Carlo radiation transport code, allows the user to simulate radiation transport and interactions of particles in a defined world. By creating a model of the GaN FinFET with a neutron conversion material, a neutron source can be simulated, where neutron transport and interactions can be tracked. Reaction products in the conversion material can then be tracked, providing information like the location, energy, and momentum of the particles. This track information can then be filtered to build a database for where

NSC-614-5769 11/2023
Unclassified Unlimited Release

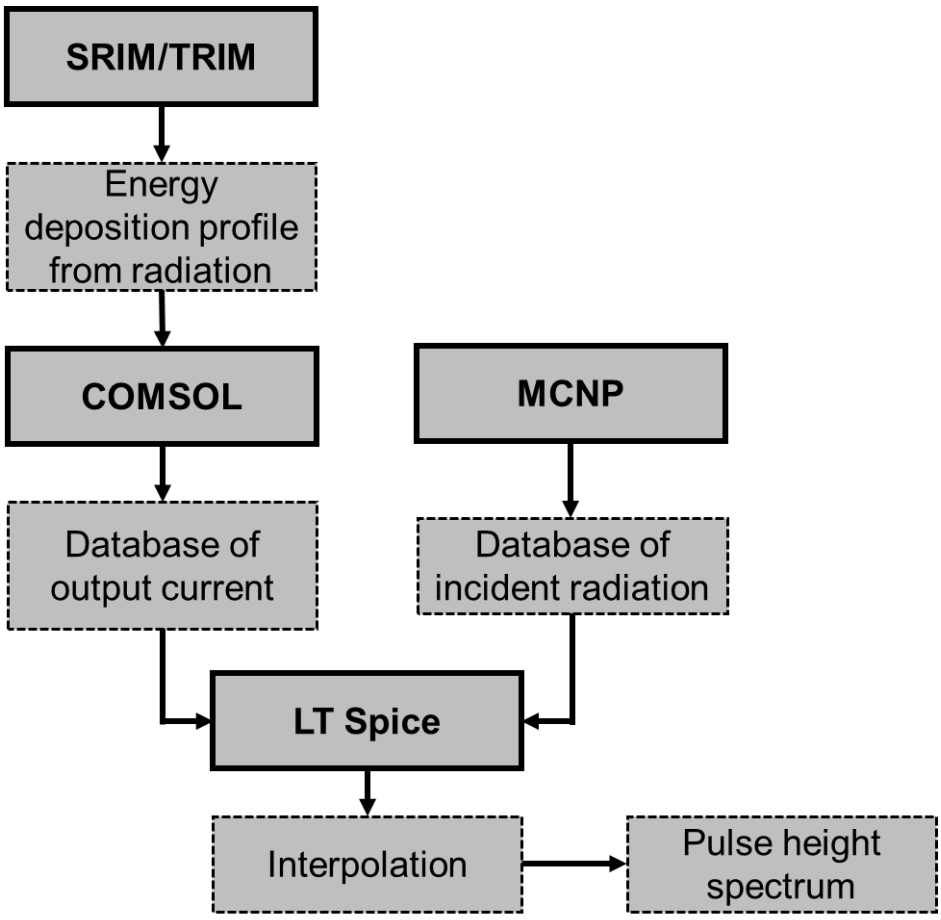

Figure 1.2: *Flowchart of simulation framework used to analyze radiation detection systems.*

directly ionizing radiation has the highest probability of contacting the modeled device. By knowing the location, energy, and momentum vectors of ions entering the modeled device, electronic charge simulation can be used to determine the device's electronic response.

Using COMSOL Multiphysics, a finite analysis solver, the GaN FinFET device's electronic characteristics can be simulated. By building a model and providing adequate physics initial and boundary conditions, electronic transport can be simulated with both static and time-dependent studies. COMSOL allows user-defined charge generation, where custom charge generation spatial distributions and rates are possible. This feature is where the database of incident ions from MCNP are utilized. A database of the device's output current response can be built. Typically, a detection system will use a charge integration circuit for the processing of a detection. Therefore, by integrating the output current responses over

NSC-614-5769 11/2023
Unclassified Unlimited Release

time, the output charge of an incident ion will be calculated, and ultimately, a database of charge for the given incident ion simulation.

Using the TRIM program in SRIM, ion transport in materials can be simulated. This program is used to support the charge generation profile in COMSOL, where the Bragg curve of the impinging ion can be imported and used as the axial shape of charge generation.

For simulation of the readout electronic circuitry, LTspice allows users to simulate circuits and import the simulated drain currents from COMSOL. For example, an ORTEC 142A preamplifier circuit may be implemented, with some estimations due to proprietary component values[21].

Because the physics of the device can be adjusted in COMSOL, tuning physics can be added into COMSOL. Some physics that can be added include custom carrier mobility models, custom trapping and recombination models, and fixed charge along boundaries. This implies that a device's output may be tuned to real hardware. This also implies that damage to the simulation model in COMSOL could be implemented by adjusting the mobility, fixed charge, or other parameters suspected.

1.3 Hardware

Various fabricated multifin samples of GaN vertical FinFETs were provided by Kyma Technologies, Inc. Shown in Fig. 1.3 are images of the devices. These devices had fin height dimensions of 1.5 µm, fin width dimensions of 100 nm, gate height up the sidewall of the fin of about 750 nm, and device pitch of either 1.1 or 1.6 µm. Select devices were tested by Kyma for the current-voltage response, with a "bad" device defined as gate leakage current greater than 10 µA. KSU also tested the devices and compared results. The family of curves, defined as the plots of the drain current versus the drain-to-source voltage for given gate-to-source voltages, were used to tune the the simulated COMSOL model. The dimensions and materials used to create the simulation models follow that of information provided by Kyma and their publication[24] as well as other GaN vertical FinFET literature[25–28], using the pitch of 1.1 µm. The materials follow that provided from Kyma shown in Fig. 1.4.

NSC-614-5769 11/2023
Unclassified Unlimited Release

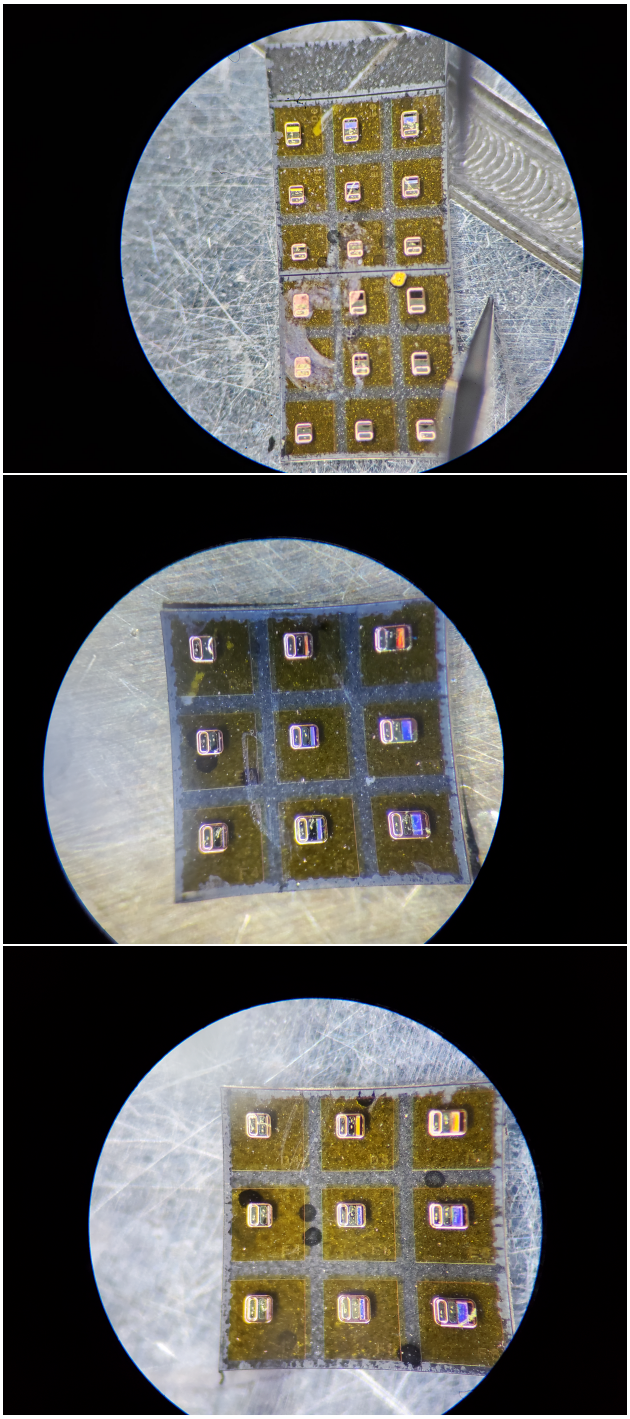

Figure 1.3: *Kyma Technologies sample FinFET devices under probe station microscope.*

The simulation models developed follow that of an ideal geometry, where the geometric values are assumed to be correct such that tuning should take place from other physics in the device rather than the geometry. Through the use of the simulation framework and

NSC-614-5769 11/2023

Unclassified Unlimited Release

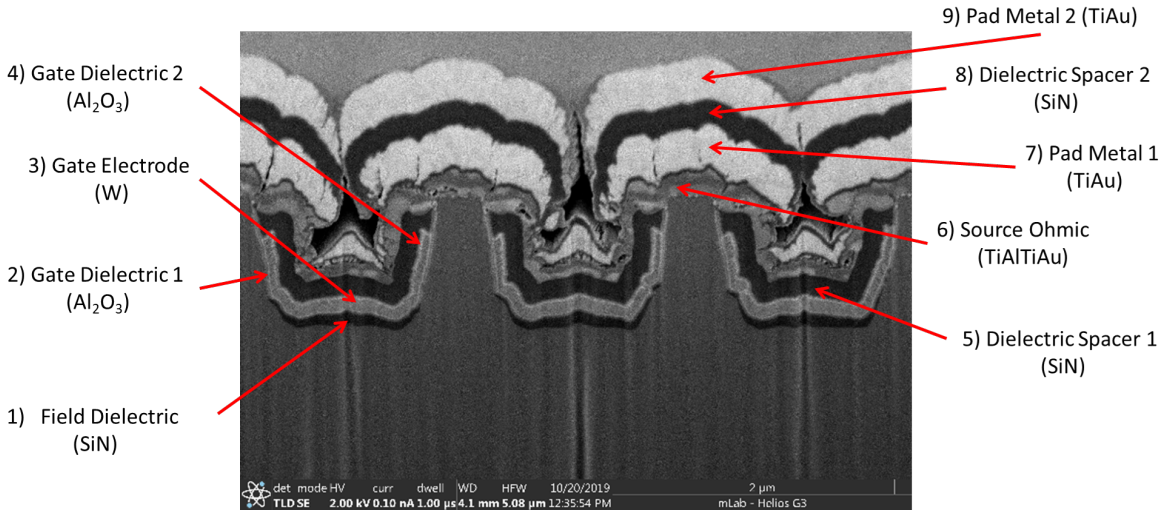

Figure 1.4: *Cross-section image of fabricated GaN FinFETs, with material annotations*[2].

hardware analysis, the basis of determining if the GaN vertical FinFET is effective as a thermal neutron detector is possible. The geometric device parameters follow that of the real samples, with dimensions and materials provided by Kyma. The neutron conversion film considered was B_4C, chosen based on literature comparing LiF and B_4C conversion films on simulated GaN planar detectors[29]. Boron reacts with a thermal neutron to yield an alpha particle and lithium ion, Fig. 1.5.

$$^{10}\mathrm{B} + ^{1}_{0}\mathrm{n} \rightarrow ^{7}\mathrm{Li}^{*}(0.840\ \mathrm{MeV}) + \alpha(1.470\ \mathrm{MeV})$$

$$^{10}\mathrm{B} + ^{1}_{0}\mathrm{n} \rightarrow ^{7}\mathrm{Li}(1.015\ \mathrm{MeV}) + \alpha(1.777\ \mathrm{MeV})$$

The lithium and alpha products will be released in opposite directions after the neutron is absorbed. The reaction also yields a 480 keV gamma ray from the excited ^{7}Li 94% of the time, while the remaining yield of 6% does not leave the ^{7}Li in an excited state[3]. The gamma ray was not considered in the radiation and electronic transport simulations, as GaN was shown to be insensitive to the gamma ray[8].

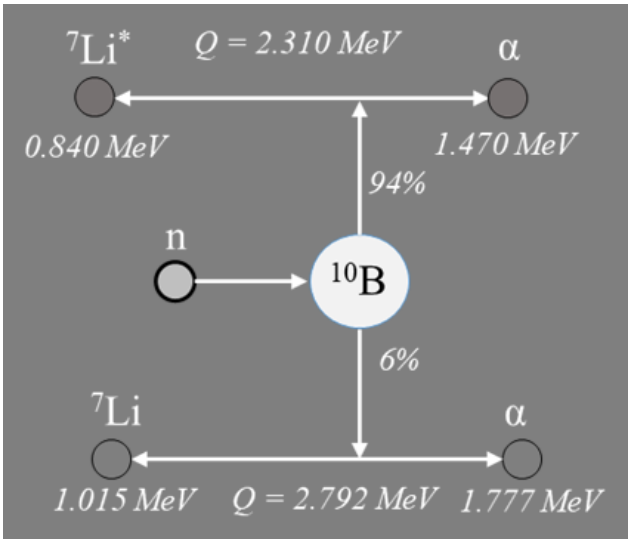

Figure 1.5: *Reaction products from neutron-boron capture reaction*[3].

NSC-614-5769 11/2023

Unclassified Unlimited Release

Chapter 2

Radiation Transport Simulation

2.1 Model

Using MCNP6, the radiation transport model of the GaN FinFET was designed using surface card planes, following the hardware dimensions for a single fin device stated in section 1.3, including materials annotated in Fig. 1.4. An illustration of the materials and model dimensions are shown in Figs. 2.1 and 2.2. The model included the dielectric SiN along the base of the trench and AlON along the edge of the fin, as well as the metal contacts, pad metals and dielectric spacers. The top-most metal padding layer was simulated as 0.5 µm thick with a dielectric spacer of 0.3 µm, followed by another metal padding layer 0.5 µm thick. The leftover space in the trench was then filled with B_4C neutron conversion material.

At the edges of the model were reflection planes. These reflection planes reflected any particles that reached them, with the goal of simulating a multifin device while only needing to model a single fin. The pitch of the device (1.1 µm) represents the bounds for a unit cell, therefore, by placing the coordinate system at the center-line of the fin and base of trench, the reflection planes were placed at +/-0.55 µm in the x direction as well as the z direction (out-of-page direction). Reflection barriers were also placed at the top and bottom of the simulated model, where the bottom reached 5 µm below the GaN trench and the top reached 0.1 µm above the thermal neutron source.

NSC-614-5769 11/2023

Unclassified Unlimited Release

The thermal neutron source was defined as an isotropic irradiating plane 0.1 cm directly above the pad metals, with the space between the metal and source defined as air, emmitting 0.0253 eV neutrons towards the FinFET. The simulated neutron source represents if the device was in close proximity to a moderated neutron source, like near a nuclear reactor or a cask of a neutron source.

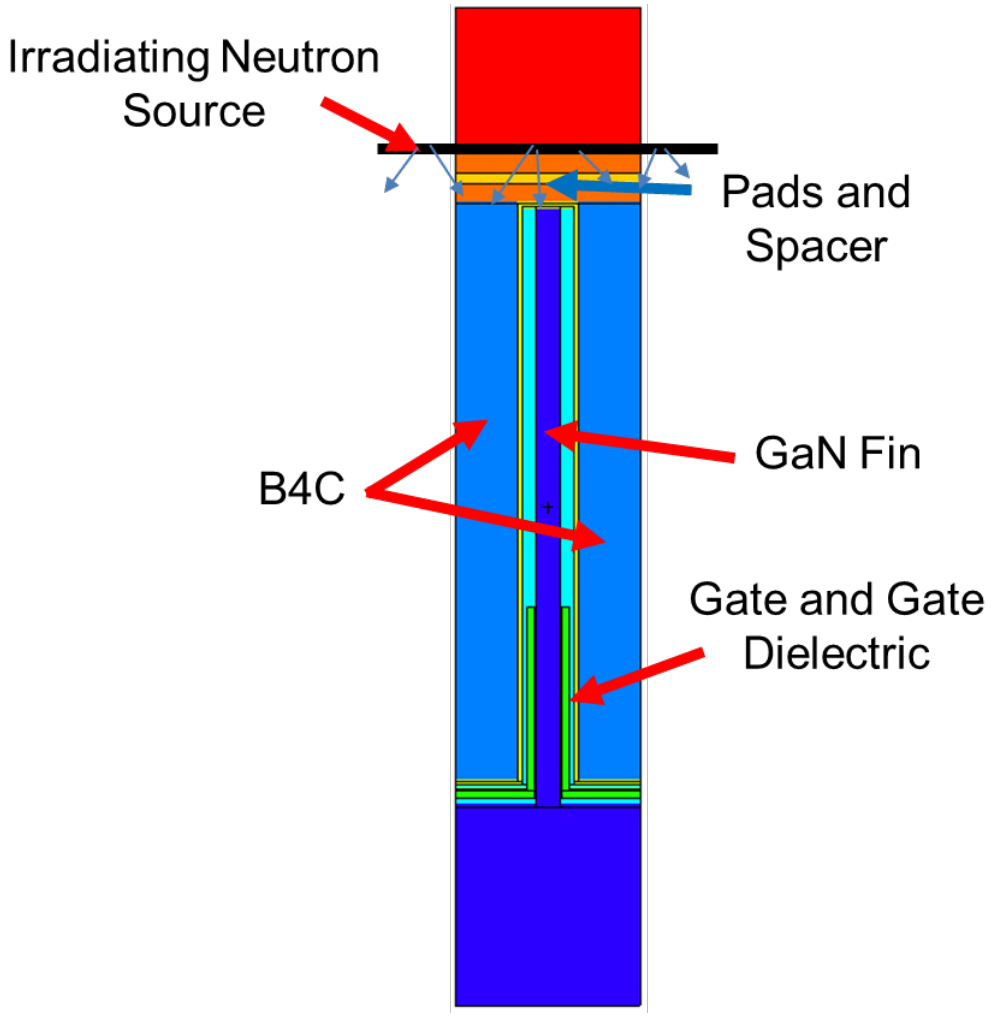

Figure 2.1: *Illustration of FinFET model and thermal neutron source placement. Not to scale.*

The particle track (PTRAC) output file option was used to allow the user to record filtered particle events, which for this work were the reaction products of lithium ions and alpha particles. The PTRAC method was used to record all surface interactions involving alpha and lithium ions for histories which passed through the GaN fin or bulk of the FinFET

NSC-614-5769 11/2023
Unclassified Unlimited Release

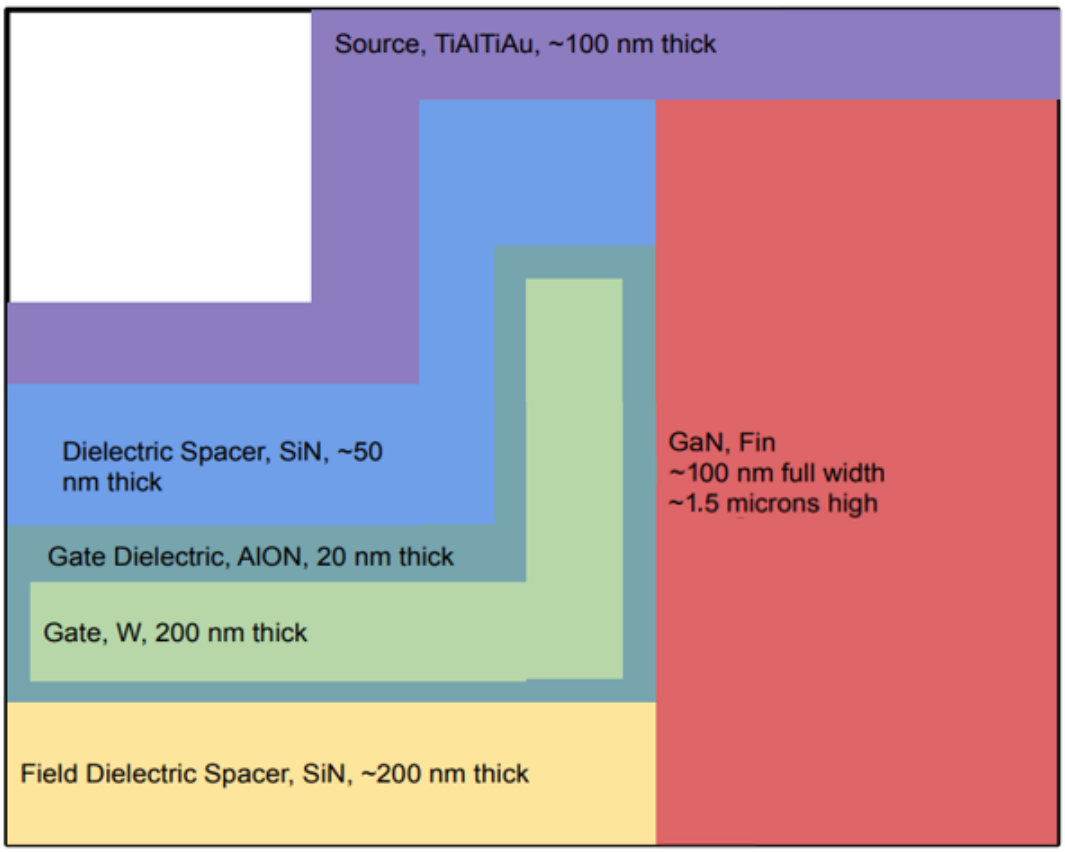

Figure 2.2: *Illustration of half of FinFET model materials and dimensions. Not to scale.*

geometry. The MCNP input file was limited to 1×10^{10} neutron histories **or** until the PTRAC output file reached 1×10^{6} step histories. The step histories means that if a reaction product particle (alpha or lithium) reached the GaN, its track history would be recorded as steps starting from where the particle was born to where it was terminated. If two reaction product particles reached the GaN, there would be two separate track histories recorded in the PTRAC output file. Through the PTRAC output, the alpha particle and lithium particle B_4C reaction products were separated and filtered to determine the location, angle, and particle energies when incident on the GaN material. By separating out the GaN geometry into two cells, the fin and the bulk, the reaction product histories were easily stored in separate databases– this was done to help process the databases for the convolution with the electronic transport database.

NSC-614-5769 11/2023
Unclassified Unlimited Release

Chapter 3

Fabricated FinFET Device Testing

Forty-five GaN vertical FinFET devices were provided by Kyma Technologies, Inc. to help tune simulations to hardware. A datasheet, provided with the devices, included 10 devices tested for current-voltage curves, where 3 devices tested were not included in the KSU devices. The equipment used in the device testing is shown in Table 3.1. The cables used include 1 triax cable, 2 BNC cables, 2 single tip cables (1 with BNC connector), and 2 BNC splitter to banana clips.

Table 3.1: *Equipment and materials used in the FinFET hardware testing.*

Component	**Model No.**	**Serial No.**	**Company**
GaN FinFETs	REVH-Q4	-	Kyma Technologies, Inc.
High Voltage Power Supply (drain, source contact)	237	861426	Keithley
High Voltage Power Supply (gate contact)	DP832	DP8C194406180	Rigol
Probe Holder (source contact)	S-725-CRM	20087189	Signatone
Probe Holder (gate contact)	S-725-CLM	06122159	Signatone
Probe Tips (1 µm tip)	SE-SMS	-	Signatone
Probe Tips (whisker tip)	SE-10T	-	Signatone
Probe Station	H100	KSU:460465	Signatone

The goal in testing the devices were to determine the output characteristics through the family of curves. The family of curves considers the current-voltage curves for different values

NSC-614-5769 11/2023

Unclassified Unlimited Release

of gate bias. These current-voltage curves provide insight on device's resistivity and electron mobility, or performance of device when used as a transistor. These output curves provide a goal for the electronic transport simulation work to help generate simulation results closer to fabricated hardware.

The testing equipment was set up following the illustration in Fig. 3.1 in order to gather the family of curves for the devices. The workstation used is shown in Fig. 3.2. To verify the equipment was set up properly, a commercial MOSFET IRL520N was tested against its specification sheet. Once the equipment was confirmed to be working correctly, the FinFET samples were systematically tested by repeating the following procedure:

1. With both voltage sources turned off, the probe tips were carefully placed onto respective contact pads and the dark box enclosure was slowly closed.

2. The gate voltage source was set to 0 V and turned on.

3. The drain voltage source was programmed to sweep from 0 V to 10 V with a +0.05 step and 0.05 second delay, where the drain current versus drain voltage was recorded on a connected computer.

4. After the sweep was recorded and saved, the process of changing the gate voltage source by 1 V increment and running the sweep was repeated.

5. After recording the drain current versus drain voltage plot for a gate voltage of 5 V, the gate source was slowly lowered back to 0 V, shut off, and the the connector to the gate voltage source was flipped to test negative voltage.

6. The recording procedure was repeated for gate bias of −1 V and −2 V (showing positive on power supply), after which the gate source was returned to 0 V, shut off, and the connector flipped back for positive gate bias.

7. The dark box enclosure lid was carefully opened and the probes were removed from the FinFET sample.

NSC-614-5769 11/2023

Unclassified Unlimited Release

After collecting the data, the family of curves could be compared to the Kyma tests as well as simulated results.

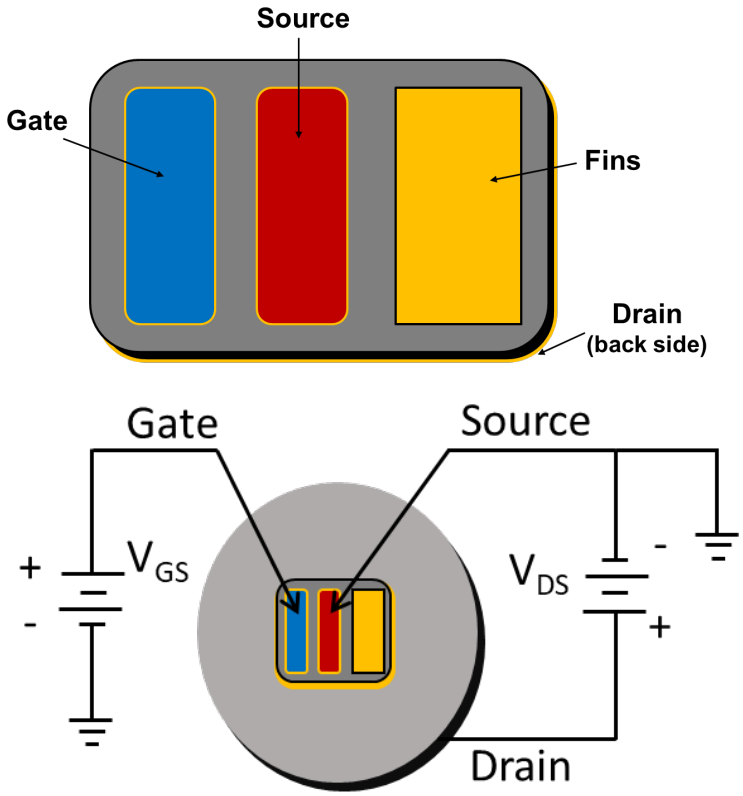

Figure 3.1: *Illustration of wiring schematic for Kansas State testing of FinFET devices*[2].

NSC-614-5769 11/2023
Unclassified Unlimited Release

Figure 3.2: *Kansas State probe station, with dark box enclosure and microscope, including the Keithley 237 High Voltage Source and computer for measurement collection.*

NSC-614-5769 11/2023

Unclassified Unlimited Release

Chapter 4

Electronic Transport Simulation

4.1 COMSOL FinFET Model

COMSOL Multiphysics is a commercial finite analysis solver that lets the user create CAD models and apply initial and boundary conditions to solve fundamental equations. The model can be either 3D or 2D, depending on the device symmetry. Because the GaN vertical FinFET is symmetric, a 2D simulation will provide a good approximation of 3D device. This implies that an out-of-plane depth is necessary to correct device output, for results like drain current. The Semiconductor Module in COMSOL lets the user implement semiconductor physics to the model, such as doping, trapping, recombination, charge conservation, and charge generation.

The model built for the GaN FinFET in COMSOL is shown in Fig. 4.1. Two materials were used in the model: GaN and AlON. The core of the device is the cross-section of the GaN FinFET, with the dielectric material AlON (relative permittivity $\epsilon_{rel} = 8.56$[30]) on the base of the trench (100 nm) and edge of the fin (20 nm), consistent with literature and Kyma information[2;31]. On top of the AlON is another layer of highly n-type doped semiconductor–this was added only so that a metal contact could be applied (metal contacts could not be applied to dielectric materials in COMSOL ver. 5.6). There are physics in the Semiconductor Module that create boundary conditions for thin insulating gates, however,

NSC-614-5769 11/2023

Unclassified Unlimited Release

it assumes only perpendicular field lines into the boundary, so at the junction of the fin and trench the simulation had a difficult time converging on a solution. The dielectric material travels above the conductive semiconductor material (gate contact) along the fin edge in order to allow electric field lines and bias to permeate to the GaN fin–this also helps with convergence on a solution as the junction of the dielectric and GaN would be abrupt. The dielectric was not modeled to the top of the device in order to keep the COMSOL model simple, using the assumption of an ideal device.

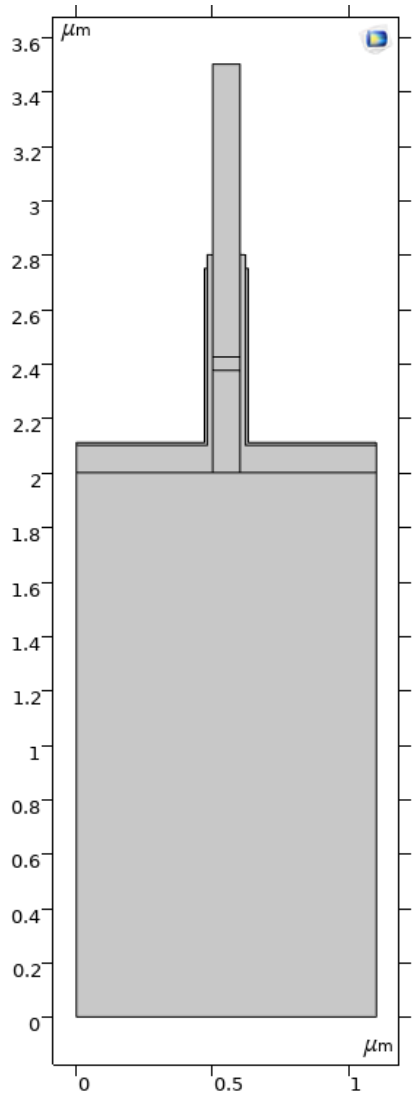

Figure 4.1: *COMSOL model of 2D GaN vertical FinFET. This model includes the charge generation domain (small domain located in the fin) with gate dielectric material and conducting semiconductor material in order to use metal gate contact physics.*

NSC-614-5769 11/2023

Unclassified Unlimited Release

The physics included in the COMSOL FinFET model are: analytical doping, geometric doping, charge conservation, heterojunction/continuity, ideal ohmic metal contacts, trap-assisted recombination, Auger recombination, and direct recombination.

The analytical doping for the model accounted for the background n-type doping of GaN with a value of $2 \times 10^{16}\,\mathrm{cm}^{-3}$. Analytic doping was also used for the semiconductor layer for the gate contact, providing a high n-type doping value of $1 \times 10^{19}\,\mathrm{cm}^{-3}$. The geometric doping is used to give a Gaussian doping distribution away from a boundary. For the GaN FinFET, the geometric doping was used on the source and drain metal contacts for high n-type doping with values of $2 \times 10^{18}\,\mathrm{cm}^{-3}$ and $1 \times 10^{19}\,\mathrm{cm}^{-3}$ respectively. The geometric doping junction length away from both the source and drain was set to 0.5 µm, which falls in line compared to literature[25].

Charge conservation physics were used to create the dielectric material between the gate contact and the GaN fin and trench. This ensures that current will not pass through the domain, but conserves electric fields from the gate to the GaN via $\mathbf{D} = \epsilon_0 \epsilon_{rel} \mathbf{E}$. Heterojunction/continuity allows the domains built to have continuous band structure based on each domain's quasi-Fermi levels, requiring the value for holes and electrons are equal at a junction.

Recombination models were added to the GaN FinFET domains through the use of Shockley-Read-Hall recombination, Auger recombination, and direct recombination. Shockley-Read-Hall recombination considers traps created in the forbidden zone, inside the band gap, by ways of impurities or defects in the crystal[32;33]. In COMSOL, electron and hole lifetimes are input, as well as the defect level. For the current study, the defect level was assumed to be 0 eV. The electron lifetime value was 0.7 ns, and the hole lifetime value was 2.0 ns as done in other literature[34]. Auger recombination was added to the GaN, which is considers recombination when like carriers collide causing one to recombine and the other to absorb the extra energy rather than radiate a photon. The Auger recombination physics requires Auger recombination factors for electrons and holes, with values of $3 \times 10^{-31}\,\mathrm{cm}^6\,\mathrm{s}^{-1}$ for both factors[34]. Lastly, direct recombination was used in the COMSOL FinFET model, where recombination is due to radiative transfer. A photon may be absorbed to create an

NSC-614-5769 11/2023
Unclassified Unlimited Release

electron hole pair and a photon may be emitted when the electron in the conduction band recombines with the hole in the valence band. In COMSOL, the recombination factor used was $1.1 \times 10^{-10}\,\mathrm{cm}^3\,\mathrm{s}^{-1}$.

Material properties of the GaN, like the electron and hole mobility, can also be manipulated to adjust the FinFET's output characteristics. Because the FinFET is n-type doped, the electron mobility will manipulate the amount of current that can reach the contacts. The electron mobility in the material properties of COMSOL were used as a simple tuning mechanism to help match the results of the fabricated hardware testing.

4.2 Meshing Techniques

In order for a finite analysis solver to work, it needs finite elements of the model. The finite elements are provided through meshing, therefore, the converged solution is highly dependent on the meshing. Large elements are suitable areas of little change in physics, and small elements are necessary for areas with noticeable change in physics. Regions in a model that require small mesh elements include areas with a gradient of doping, junctions, corners, and active regions where electric potential will change. Small elements will also be needed to simulate a charge generation profile, as there will be noticeable change in the generation profile in space.

COMSOL recommends the use of a structured mapped meshing for solving semiconductor simulations, as it can use a more efficient finite volume solver versus a finite element solver. The structured mesh can be applied to the GaN FinFET model, however, when it comes to generating charge to simulate an incident ion, the structured mesh cannot be used. This is because the mapped mesh requires that all elements to match adjacently, and when simulating an ion entering at any non-perpendicular angle no longer will the elements be matched to one another. Instead a triangular mesh is used throughout the device, with size emphasis on the fin region, the source contact, and the drain contact. An example of the meshing of the generation domain for the time-dependent studies is shown in Fig. 4.2.

NSC-614-5769 11/2023
Unclassified Unlimited Release

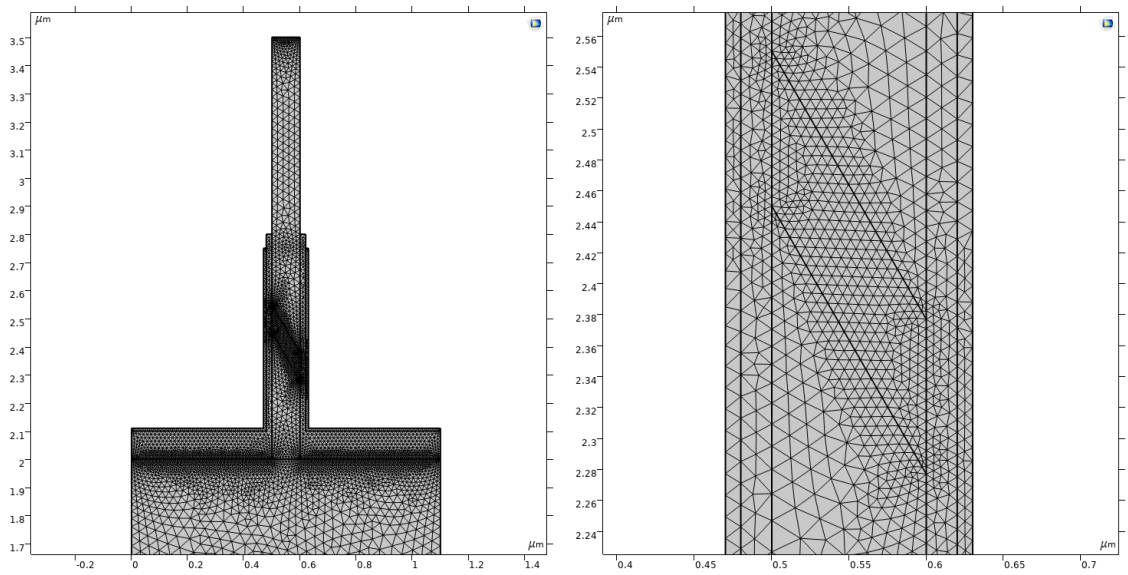

Figure 4.2: *The meshing used for time-dependent solutions, zoomed out (left) and focused on the generation domain (right). In order to converge on a solution in COMSOL, the meshing must match the physics.*

4.3 Particle Ionization Simulation

When a charged particle passes through GaN, electron hole pairs are created, with an average ionization energy of approximately 10 eV. The charged particles of interest for the boron neutron capture reaction are the alpha particles and lithium ions. There are two yield branches to the reaction, with a 6% probability of 1015 keV lithium ion and 1777 keV alpha particle products, and a 94% probability of 840 keV lithium ion and 1470 keV alpha particle products.

The charged particles lose energy along their track length through the GaN as they ionize the medium. The energy loss rate as a function of the particle distance through the medium is called the Bragg curve. While Bragg curves vary from particle to particle and energy to energy, the Bragg curve shape tends to repeat itself for the same particle with varying energy. This means a Bragg curve of a higher energy particle can be transformed into a Bragg curve of a lower energy particle, given they are the same particle and traveling through the same medium. Because the Bragg curve gives a 1-dimensional look at the energy lost in the GaN, it is used as the axial spatial profile to generate charge (electron hole pairs) in the device.

NSC-614-5769 11/2023

Unclassified Unlimited Release

The Bragg curve for the 1777 keV alpha particle through GaN is shown in Fig. 4.3.

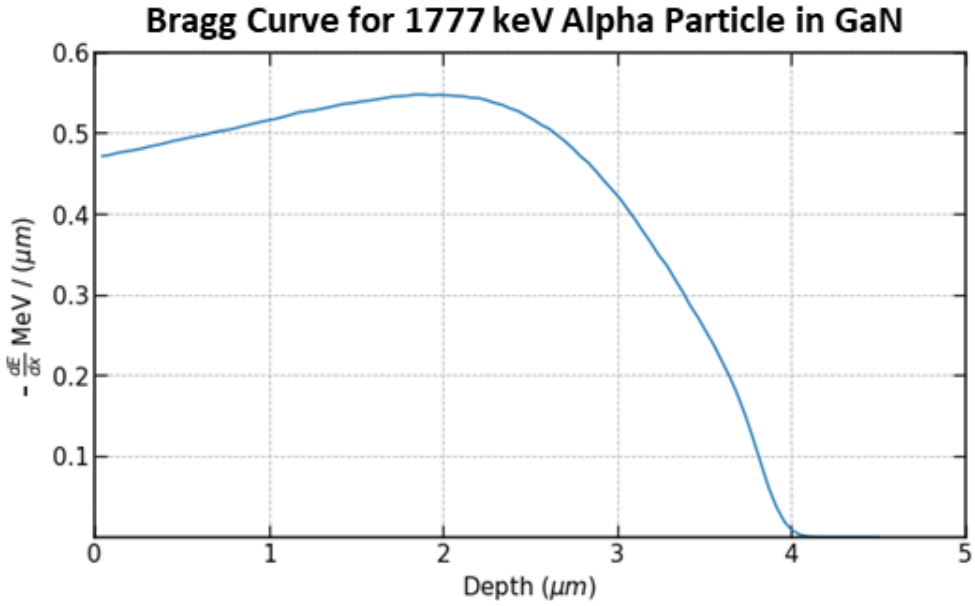

Figure 4.3: *Bragg curve for* 1777 keV *alpha particle traveling through GaN, calculated from SRIM/TRIM.*

The Bragg curve for alpha and lithium particles is calculated using TRIM. By simulating 10,000 normally incident 1777 keV helium ions and 1015 keV lithium ions into a 5 µm GaN layer, the Bragg curves are recovered from the ionization plots. The Bragg curves are verified by integrating over the particle range to recover a value that is near the starting energy (not all of a particle's energy will be lost to ionization). The Bragg curves can then be imported into COMSOL to be used as the axial charge generation profile.

While it is hard to determine the size of an ionization cloud, it is assumed that the ionization cloud should be small around the particle's track. Using a Gaussian profile as the radial charge generation profile, the charge cloud is limited to a radial width of 50 nm. Because there is a gradient implemented into the semiconductor physics, small mesh elements are required in the the generation zone. The size of the mesh elements are chosen based on their ability to reduce skewed triangles in the meshing in the generation zone as well as the area around, and adequately render the generation profile. Increasing the number of mesh elements also increases the workload of the computer and ultimately affects simulation times.

NSC-614-5769 11/2023
Unclassified Unlimited Release

With the spatial profile implemented into COMSOL simulating the energy loss of the particle, the time aspect of the charge generation also needs to simulate an ionization event. It is assumed that an ionization event happens nearly instantly, however, reasonable limitations are necessary to ensure COMSOL can converge on a time-dependent solution. The time profile $T(t)$ used to turn on and off the generation of electron hole pairs in COMSOL follows a normalized error function.

The temporal function is given as

$$T(t) = \frac{2\exp\left[-(\frac{t-T0}{TC})^2\right]}{TC \cdot \sqrt{\pi}\mathrm{erfc}(-\frac{T0}{TC})}, \tag{4.1}$$

where t is time, *erfc* is the complementary error function, the parameters $T0$ and TC control when the peak value value occurs and the width of the distribution respectively, and has units of s^{-1}. The time profile has an on-range of approximately 0.4 ns, and works with COMSOL.

The electron hole pair generation domain created in COMSOL allows the user to give the particle, energy, location, and incident angle and automatically translate, rotate, and implement the correct generation profile in the domain. The translation and rotation aspect was implemented through a rotational matrix that adjusts the radial (r) and axial (l) distance components of the domain and generation profile. This is done by transposing the system so that the center of the new coordinate system, P_o, is the point where the user desires the particle path to begin and is given in the original x and y coordinate system.

$$P_o = \begin{bmatrix} P_{o,x} \\ P_{o,y} \end{bmatrix}$$

Consequently l and r are calculated by

$$\begin{bmatrix} r \\ l \end{bmatrix} = \begin{bmatrix} \cos(\theta) & \sin(\theta) \\ -\sin(\theta) & \cos(\theta) \end{bmatrix} \cdot \begin{bmatrix} x - P_{o,x} \\ y - P_{o,y} \end{bmatrix}$$

NSC-614-5769 11/2023

Unclassified Unlimited Release

The r and l distances are then implemented into the axial $A(l)$ and radial functions $R(r)$. The radial model $R(r)$ is given as

$$R(r) = \exp\left(-\left(\frac{r}{\sqrt{2}W_x}\right)^2\right), \tag{4.2}$$

with W_x controlling the decay of the Gaussian, where a value of 0.01 µm was used, and the function is unitless. The axial model $A(l)$ is given by the imported Bragg curve, where the units may be ignored or normalized.

The parameter that is then fed to COSMOL user-defined generation $G0$ is a volumetric generation rate ($\mathrm{cm}^{-3}\,\mathrm{s}^{-1}$), therefore, the out-of-plane distance d must be used. This makes the assumption that the charge generated will be uniformly spread in the out-of-plane dimension. The out-of-plane value for the simulations was 1 µm. The generation parameter goes as:

$$G0(r, l, t) = N\ R(r)A(l)T(t) \tag{4.3}$$

where r and l are functions of position and angle. The axial function $A(l)$ is also dependent on the particle type and particle energy. The variable N normalizes the spatial functions ($R(r)A(l)$), including the out-of-plane depth d, and ensures the correct number of electron hole pairs are generated.

In order to ensure the correct number of electron hole pairs are being generated in COMSOL, the charge generation spatial profile ($R(l)A(l)$) is normalized so that the number of electron hole pairs expected in a full energy deposition can be associated for the spatial profile. Then, when the spatial profile is not a full energy deposition, the fraction of the profile that is used directly scales the number of electron hole pairs generated. The expected number of electron hole pairs to generate over the full spatial profile N (including the out-of-plane depth d) is calculated by taking the particle energy E and dividing by the average ionization energy ω and the spatial profile integrated over all space:

NSC-614-5769 11/2023

Unclassified Unlimited Release

$$N = \frac{E}{\omega \int\int\int R(l)A(l)\ d\ dV}, \tag{4.4}$$

with units of cm^{-3}.

To change the axial function $A(l)$ with a change in energy, the assumption of a similar Bragg curve for lower energy like-particles is used, where the starting point of the Bragg curve is adjusted to the corresponding energy. Using a cumulative integrated Bragg curve (see Fig. 4.4), the energy of the particle is related to the distance that the particle has made it in the material to have that energy. Therefore, when given a particle energy, the new starting point of the Bragg curve on the x-axis is chosen. When a new Bragg curve is used for the axial profile $A(l)$, a new value of N must be calculated in order to normalize the full spatial profile. This is done in COMSOL by calling a database of pre-integrated spatial profiles, and interpolating where necessary.

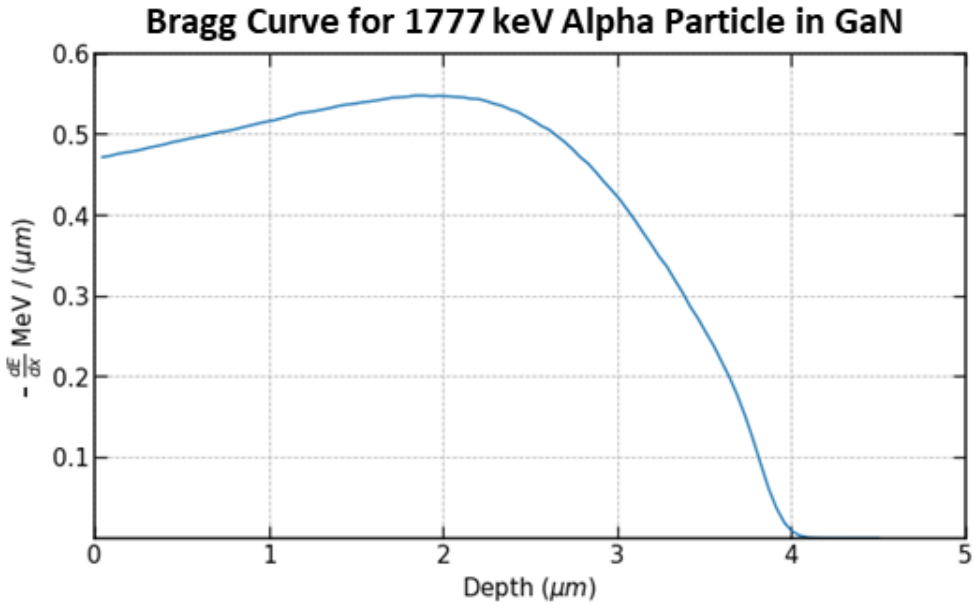

Figure 4.4: *Cumulative Bragg curve for* 1777 keV *alpha particle traveling through GaN, calculated from SRIM/TRIM and numerically calculated using Python.*

The number of electron hole pairs that were generated in COMSOL was checked by integrating the value of the charge generation parameter $G0$ over the spatial domain of

NSC-614-5769 11/2023
Unclassified Unlimited Release

the device (including the uniform out-of-plane depth d) at each time interval of the time-dependent study and integrating over each time step using Python trapezoidal integration. In equation form:

$$\text{Simulated EHP} = \int \left(\int \int \int R(l)A(l)\ d\ dV \Big|_{t_i} \right)\ dt \tag{4.5}$$

where the t_i represents each time step made in the simulation, and the integration over time was done numerically. This value was then compared to an expected value of electron-hole pair generation based on the particle track length in the GaN. The track length could be calculated through simple trigonometry by knowing the location and angle of the particle entry and using the boundaries of the FinFET geometry to know where it exited. Using the track length the expected value of electron hole pairs was calculated by integrating the Bragg curve of the given particle and energy over the calculated track length. By integrating the Bragg curve, the amount of energy the particle lost in the GaN is known. Dividing by the average ionization energy value (10 eV), the expected number of electron hole pairs is calculated. In equation form, the expected number of electron hole pairs to be generated based on a given track length L and average ionization energy ω:

$$\text{Expected EHP} = \frac{L}{\omega} \tag{4.6}$$

The methods presented in this section allow the user to simulate the ionization from a single incident ion in the GaN FinFET model. The user can choose the particle, the energy, the incident location, and the incident angle to simulate. By building up a database of single event responses, the results of the radiation transport database of incident radiation can be used to build an expected output spectrum and help characterize the device for thermal neutron detection.

NSC-614-5769 11/2023

Unclassified Unlimited Release

Chapter 5

Results

5.1 Radiation Transport Results

After running the MCNP simulation, 5,517,789 source thermal neutrons were simulated, and the output PTRAC file was processed. The PTRAC output allowed 1,000,000 step histories, and provided the particle type, location, momentum cosines, and energy for each step. Processing the PTRAC file, it was calculated that 45,229 reaction product particles reached the GaN. The file was parsed to gather only the incidences that are entering the GaN fin or trench edge by knowing the location and momentum vectors– this removes the history steps that are recorded on the interior cell boundary and on the top edge of the fin. Using the processed and filtered file of the histories incident on the fin edge and trench, histograms of the incident energies for the alpha and lithium particles were made, shown in Figs. 5.1 and 5.2. Histograms of where the particles were incident on the fin edge and trench edge were also made, shown in Figs. 5.3, 5.4, 5.5, and 5.6. The value of N shown on the histogram figures is the number of instances the reaction product particles entered the GaN, not the number of neutrons– this number can be greater than 45,229 because a single particle can be incident on the GaN edge more than once due to the reflection barriers or particles traveling through the fin and entering the bulk.

The histograms of the alpha and lithium energies (Figs. 5.1 and 5.2) show the two yield

NSC-614-5769 11/2023

Unclassified Unlimited Release

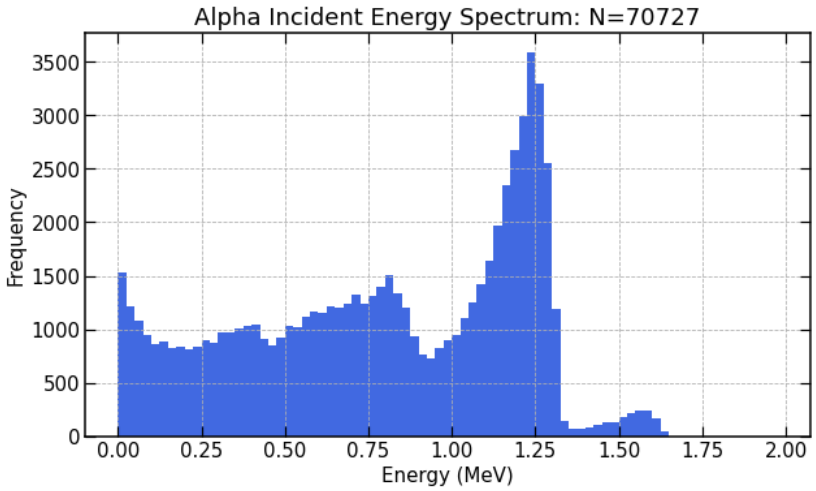

Figure 5.1: *Histogram of energy values of alpha particles incident on GaN.*

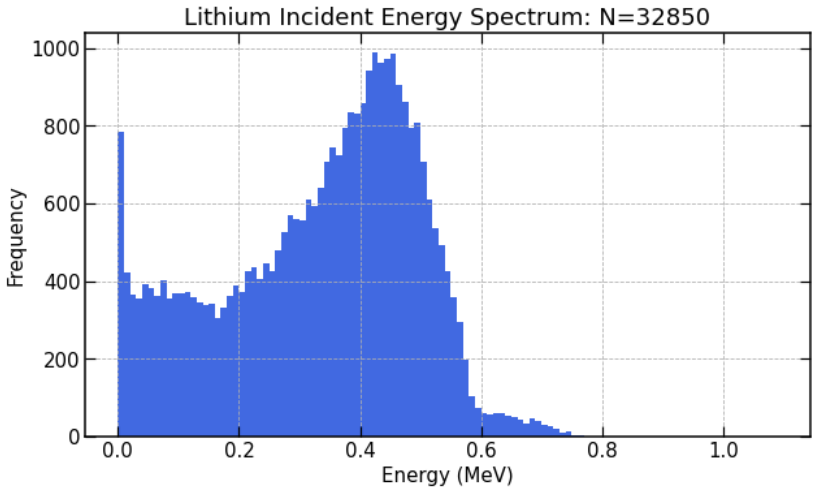

Figure 5.2: *Histogram of energy values of lithium ions incident on GaN.*

branches of the boron-neutron capture reaction by the ratio of the highest energy peak to the most frequent energy peak. For the alpha energy spectrum, the ratio is approximately $250/3500 = 7.1\%$, and the lithium energy spectrum ratio is approximately $50/950 = 5.2\%$. The most frequent energy is due to most frequent particle energy from the boron-neutron capture reaction. In the alpha energy histogram the most frequent energy is 1.24 MeV, a 0.23 MeV shift lower than the most frequently born alpha energy. The most frequent energy

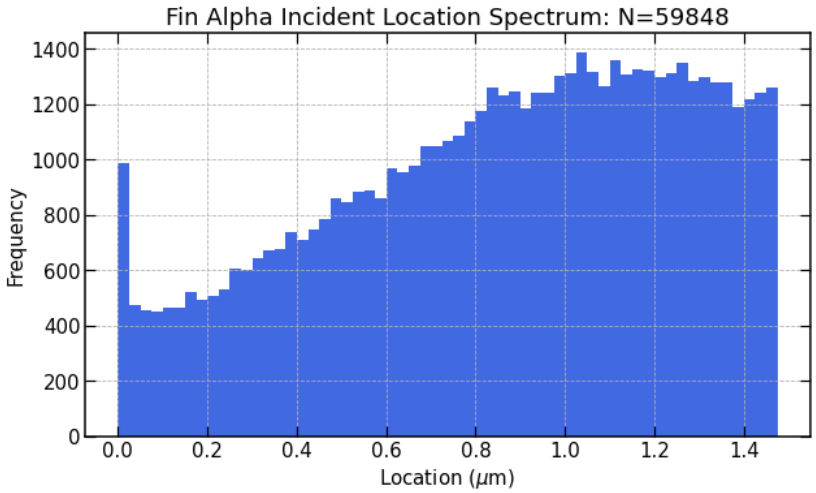

Figure 5.3: *Histogram of location values of incident alpha particles along the fin edge. Arc length of* 0 µm *corresponds to bottom (drain) of the device and arc length of* 3.5 µm *corresponds to the top (source) of the device.*

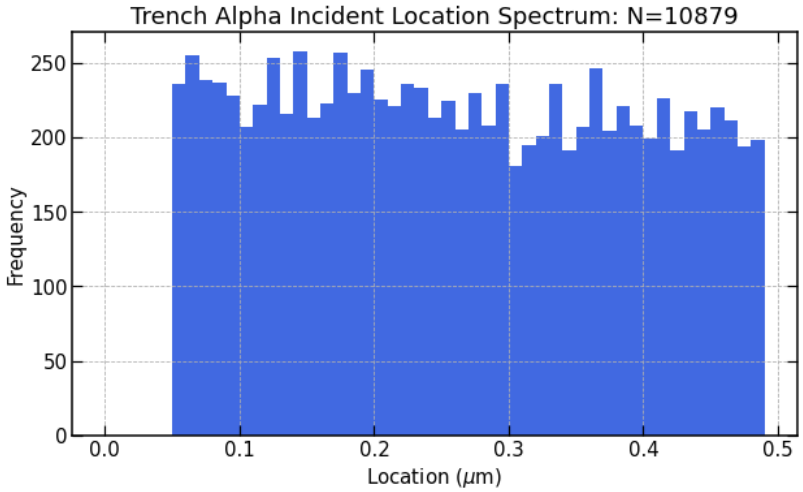

Figure 5.4: *Histogram of location values of incident alpha particles along the base of the trench. Arc length of* 0 µm *corresponds to bottom (drain) of the device and arc length of* 3.5 µm *corresponds to the top (source) of the device.*

for the lithium energy histogram is 0.42 MeV, a 0.42 MeV shift lower than the most frequent born lithium energy. These shifts represent the energy lost in the process of reaching the device edge.

NSC-614-5769 11/2023
Unclassified Unlimited Release

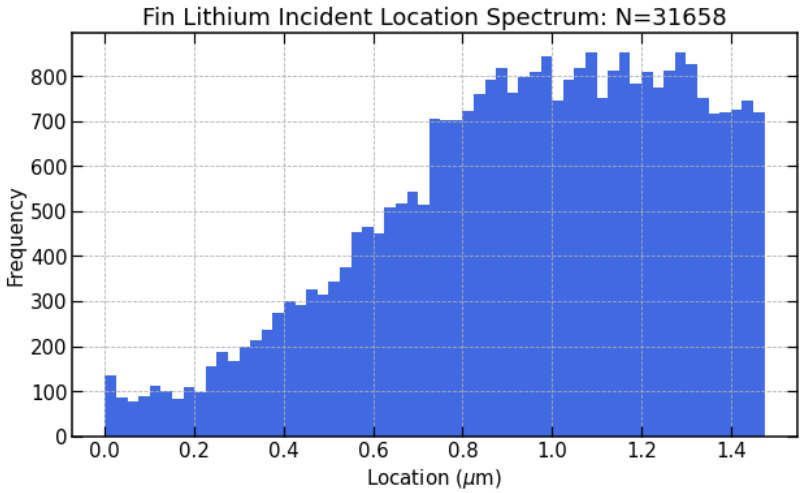

Figure 5.5: *Histogram of location values of incident lithium ions along the fin edge. Arc length of* 0 µm *corresponds to bottom (drain) of the device and arc length of* 3.5 µm *corresponds to the top (source) of the device.*

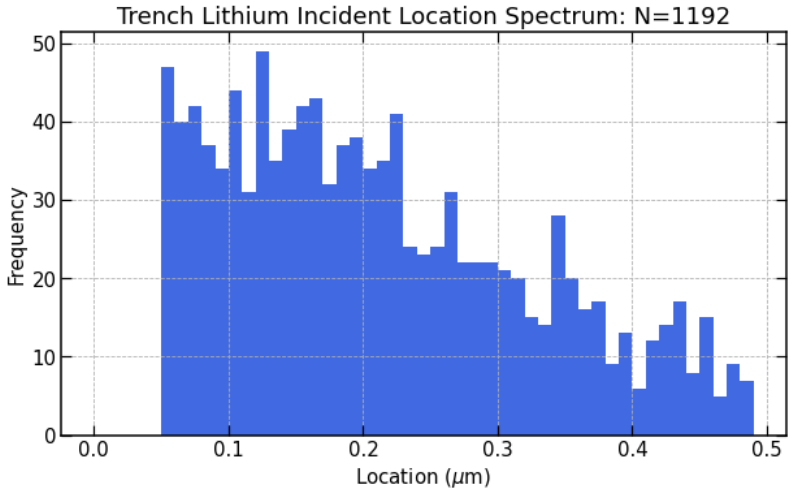

Figure 5.6: *Histogram of location values of incident lithium ions along the base of the trench. Arc length of* 0 µm *corresponds to bottom (drain) of the device and arc length of* 3.5 µm *corresponds to the top (source) of the device.*

The histograms of particle locations show that the most common location for the particles to enter the device are along fin edge, near the top of the device. This makes sense as the neutrons are irradiated from above and have a better chance of reacting with the boron near

NSC-614-5769 11/2023
Unclassified Unlimited Release

the top of the device. Another reason is that the trench base is intrinsically shielded from charged particles due to the dense tungston gate contact and dielectric spacers. There is noticeable shielding of the lithium ions compared to the alpha particles along the base of the trench, with a difference of particle instances on the base of trench of 9,687 more for alpha. There were 70,727 alpha particle incidences and 32,840 lithium ion incidences on the device edge (the sum of the incident values is over 45,229 due to reflection barriers and particle scattering).

5.2 Fabricated FinFET Device Tesing Results

A comparison of some of the tested devices from Kyma and KSU are shown in Figs. 5.7, 5.8 and 5.9. There are discrepancies in the family of curves, from the turn-on bias, on resistance, and saturated current values. These discrepancies could be there for a number of reasons, like temperature of device during testing, weak contact to terminals, or excess gate leakage current. However, on a per-fin basis, the devices appear to output inconsistent saturated current values, even from the values tested by Kyma. This makes the goal of tuning the simulated GaN FinFETs to the fabricated FinFETs difficult.

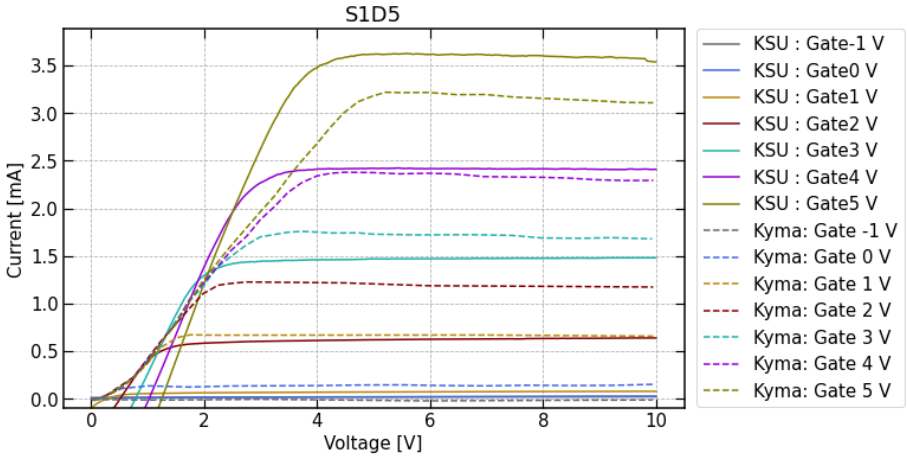

Figure 5.7: *Comparison of fabricated GaN FinFET S1D5 measured family of curves, Kyma Technologies and KSU.*

NSC-614-5769 11/2023
Unclassified Unlimited Release

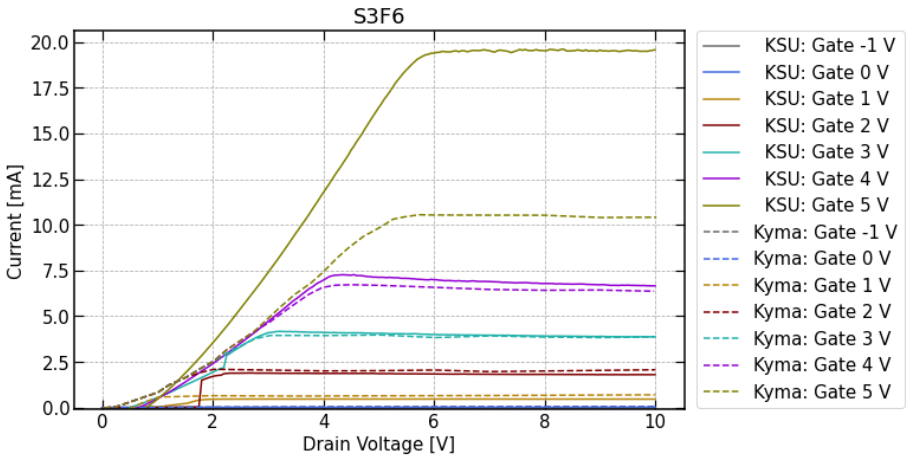

Figure 5.8: *Comparison of fabricated GaN FinFET S3F6 measured family of curves, Kyma Technologies and KSU.*

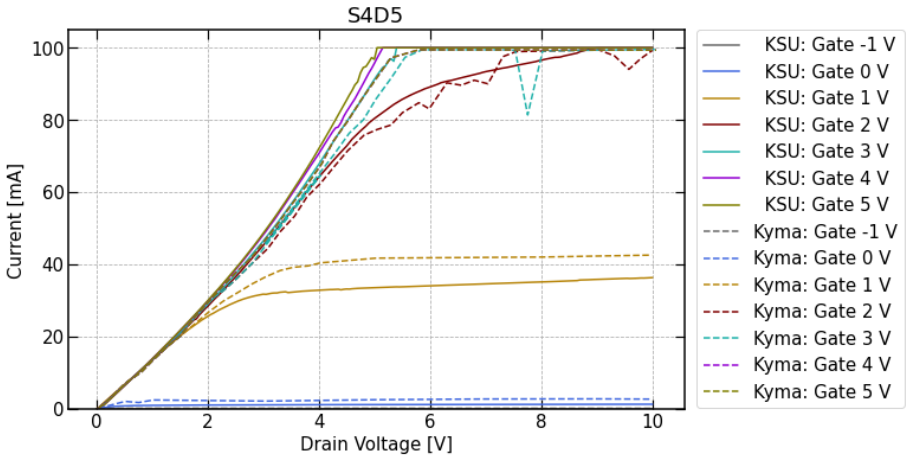

Figure 5.9: *Comparison of fabricated GaN FinFET S4D5 measured family of curves, Kyma Technologies and KSU.*

5.3 Electronic Transport Results

Two types of studies were done in COMSOL using the GaN FinFET model: the stationary study and the time-dependent study. The stationary study looked at the electrostatics of the device at different operating settings, and the time-dependent study looked at the change in the device's output from the radiation particle simulation. The stationary studies were done in forward bias to tune the COMSOL model to the fabricated FinFETs. An example

NSC-614-5769 11/2023
Unclassified Unlimited Release

of the family of curves obtained from the model is shown in Fig. 5.10. Unfortunately, there were many discrepancies when comparing the Kyma test family of curves to the KSU test family of curves, as well as inconsistencies on a per-fin basis of the saturated output current from device to device. It was clear, however, that the simulated output current was greater than the fabricated devices, so some tuning could be done to bring the current down and reach a current in the range of some of the tested devices. Shown in Fig. 5.11 are two KSU measured current-voltage curves at gate bias of 3 V and the effects of changing the GaN material electron mobility value, where a value of $200\,\mathrm{cm^2\,V^{-1}\,s^{-1}}$ falls in line with the fabricated devices. The electron mobility value of $200\,\mathrm{cm^2\,V^{-1}\,s^{-1}}$ was then used for the time-dependent studies. Off state plots of the electric potential, hole concentration, and electron concentration are shown in Figs. 5.12.

The y-component of the electric field from a center cutline of the off state device, for gate bias of $-5\,\mathrm{V}$ and $-0.3\,\mathrm{V}$, is shown in Fig. 5.13. For use as a radiation detector, the electric field should all point in the same direction, but that does not occur in the FinFET geometry without the device being in an on state. The on state does work well for radiation detection due to the large output current masking the ionization from charged particles. The best case then is to operate the FinFET at an off state closer to a gate bias of 0 V to ensure minimal background current and lower the opposing electric field at the top of the gate. Therefore, a gate bias of $-0.3\,\mathrm{V}$ was used for the time-dependent studies. Because one of the advantages of a solid-state detector is to have lower operating biases, the drain bias was increased enough to where the electric fields at the base of the fin reached electron saturation velocity for GaN[35]. This was reached at a drain bias of 5 V, with a peak electric field of approximately $1.45 \times 10^5\,\mathrm{V\,cm^{-1}}$. The operating parameters for the off state time-dependent studies were then set as: V_S =0 V, V_G =−0.3 V, and V_D =5 V with the GaN material electron mobility adjusted to $200\,\mathrm{cm^2\,V^{-1}\,s^{-1}}$.

The time-dependent studies were set up to simulate alpha particles and lithium ions at discrete locations and angles along the fin and trench edge. Due to symmetry, the simulation locations only needed to be completed on one half of the device. The locations of the simulated ions along the device edge are shown in Fig. 5.14, which includes 5 locations along

NSC-614-5769 11/2023
Unclassified Unlimited Release

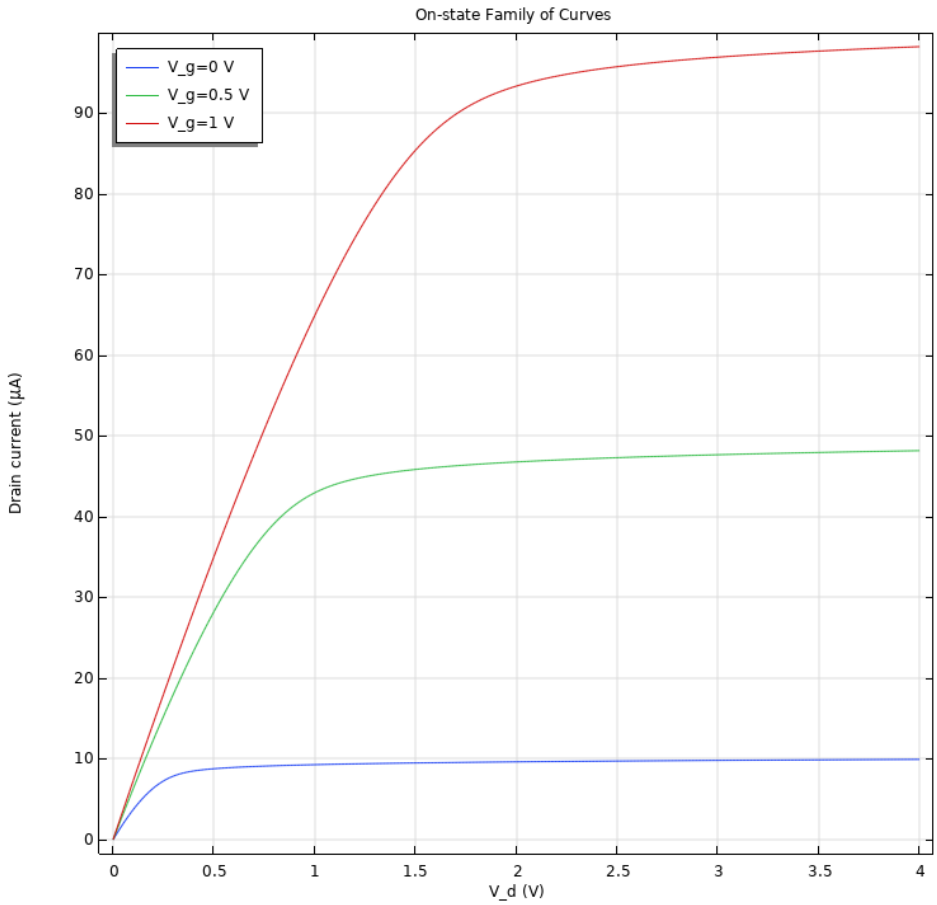

Figure 5.10: *By keeping the gate bias constant and sweeping the drain bias, a family of curves is simulated in COMSOL.*

the edge of the fin and 4 locations on the base of the trech. Each location along the edge of the fin included 9 angles of incidence, $-80°$, $-60°$, $-40°$, $-20°$, $0°$, $20°$, $40°$, $60°$, and $80°$ with $0°$ being normally incident. Each location along the base of the trench included 5 angles of incidence, $-30°$, $-60°$, $-90°$, $-120°$, and $-150°$, with with $-90°$ being normally incident to the base of the trench.

COMSOL files were set up to simulate 2-3 different particle energies at a time. The energies tested for the alpha particles incident on the base of the trench were: 50 keV, 200 keV, 500 keV, 800 keV, and 1300 keV. The energies tested for the alpha particles incident on the edge of the fin were: 50 keV, 200 keV, 500 keV, 800 keV, 1300 keV, 1400 keV, and 1700 keV. The energies tested for the lithium ions incident on both the base of the trench

NSC-614-5769 11/2023
Unclassified Unlimited Release

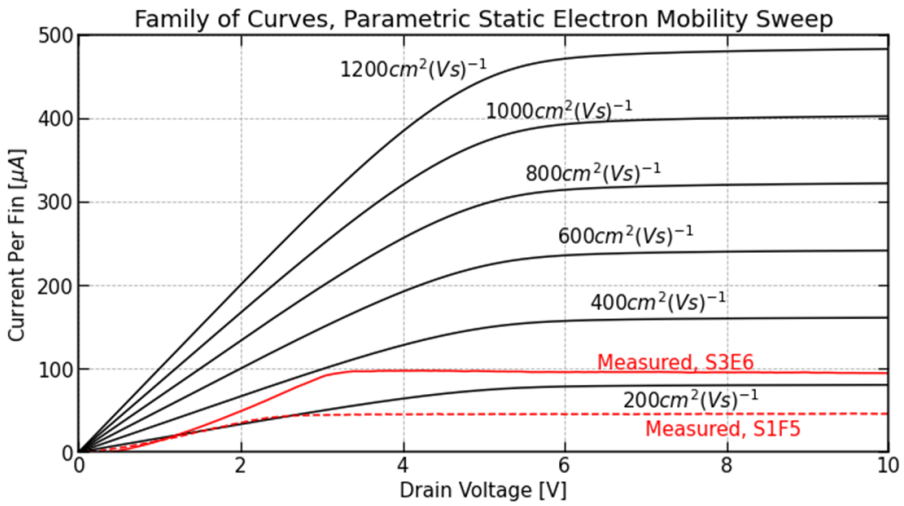

Figure 5.11: *By changing the static electron mobility in the COMSOL simulation model, the current-voltage curve (black) can be adjusted to match measured devices (red). Gate bias of* 3 V*.*

and the edge of the fin were: 50 keV, 100 keV, 200 keV, 300 keV, 500 keV, 800 keV, and 1000 keV. The time-dependent study was set up have a 0.5 ps time step during charge generation starting at time 1.9 ns to 2.1 ns. After the generation period, the time stepping was increased to 1 ps, then to 10 ps, 100 ps, and 500 ps starting at 10.5 ns where it ends at 30 ns.

The time dependent studies used the same meshing for both alpha and lithium simulations. Occasionally, convergence errors in the simulations would occur and minor adjustments to the meshing of the generation domain would typically fix the issue. When the simulations were completed, the output drain current versus time for each location and angle was exported and saved, building the database of the device responses. The current pulses were then integrated over time to calculate the induced charge (that may be collected on a charge amplifier), turning the current response database into an induced charge database.

An example of the electron and hole concentration changes over time are shown in Fig. 5.15. The output current pulse is then shown in Fig. 5.16, where the time of charge injection is centered around 2 ns. The drift and diffusion components of the output current pulses are noticeable. Because there are still opposing y-component electric fields and dead

NSC-614-5769 11/2023
Unclassified Unlimited Release

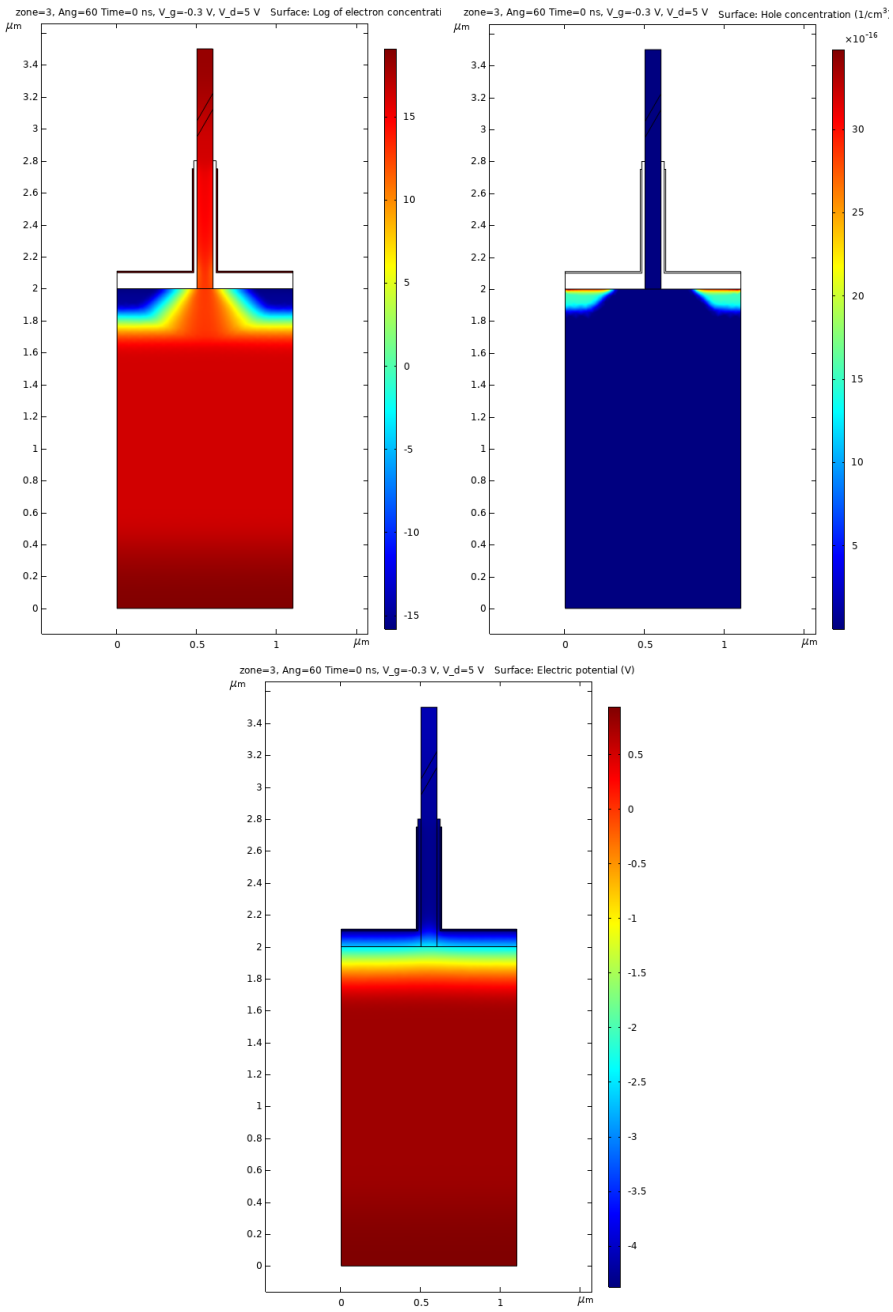

Figure 5.12: *COMSOL stationary results showing the the electron concentration, hole concentration, and electric potential for the off state GaN FinFET.*

regions, the holes find themselves stuck in the gate region and slowly recombine. The electrons are responsible for the sharp peak in the current and quickly drift, while the long tail in the pulse is from the holes slowly sweeping out of the gate region in the fin.

NSC-614-5769 11/2023

Unclassified Unlimited Release

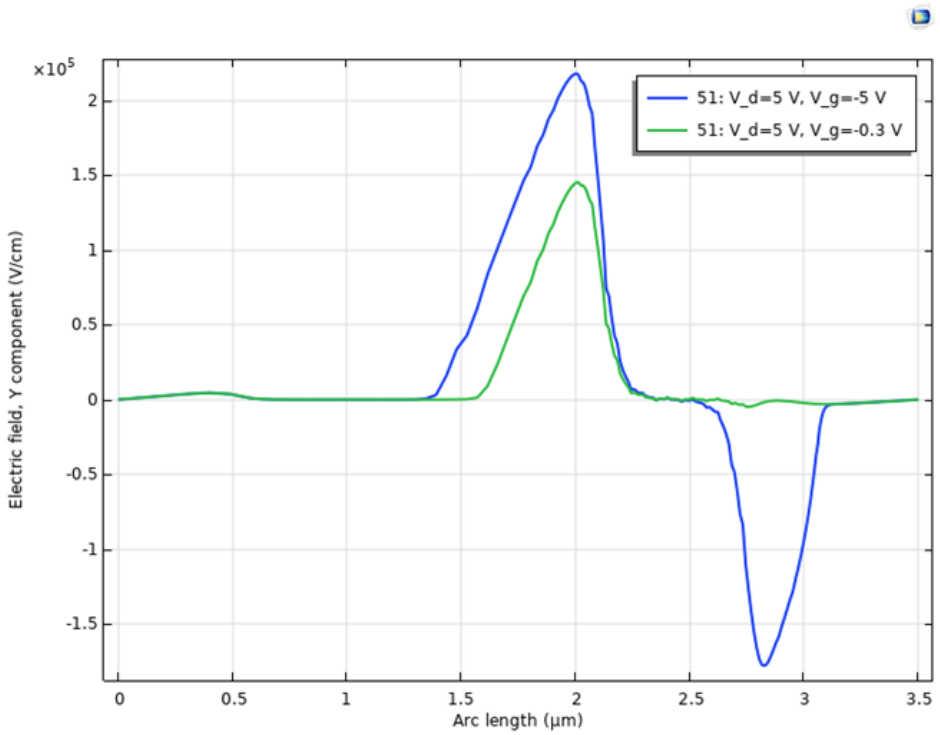

Figure 5.13: *Comparison of y-component of electric field down center cutline of GaN FinFET simulation for gate bias of* $-0.3\,\mathrm{V}$ *and* $-5\,\mathrm{V}$*, with a constant drain bias of* $5\,\mathrm{V}$*. Arc length of* $0\,\mu\mathrm{m}$ *corresponds to bottom (drain) of the device and arc length of* $3.5\,\mu\mathrm{m}$ *corresponds to the top (source) of the device.*

5.4 Combined Radiation and Electronic Transport Results

By combining the databases from the radiation transport results with the electronic transport results, an integrated charge spectrum can be built. The database from the radiation transport included histories of particles incident on the edge of the device. Because the device is symmetrical, the incidences on one half of the edge of the device were flipped on the x-location value and x-momentum value in order to match up with the integrated charge database. Clearly, a finite number of incident particle locations and angles were simulated in COMSOL and the radiation transport database includes many incident values that do not match the COMSOL half. To deal with this, linear interpolation is used.

Given a particle type, energy, location, and incident angle from the radiation trans-

NSC-614-5769 11/2023
Unclassified Unlimited Release

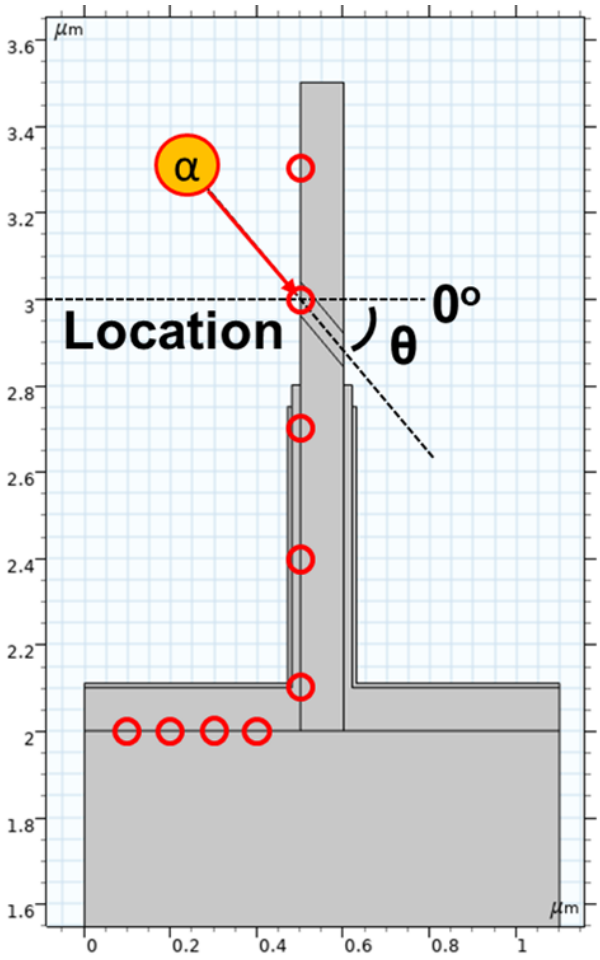

Figure 5.14: *Location of where incident particles are simulated in COMSOL. Note the angles given are referenced according the perpendicular of the side of the fin edge.*

port database, the two nearest corresponding energies are chosen in the electronic transport database. If the given particle energy is greater than the maximum simulated energy or lower than the minimum simulated energy, the value of the simulated maximum or minimum energy is used. Next, linear interpolation of the integrated charge value between the two nearest angles is determined (edge cases also use the nearest angle value), and linear interpolation of the integrated charge value at the two nearest locations follows (edge cases also use the nearest location value). Examples of the linear interpolation of the integrated charge between angles are shown for alpha particle simulations in Fig. 5.17 and for lithium ions in Figs. 5.18.

The integrated charge spectrum for alpha and lithium ions was then calculated, shown in

NSC-614-5769 11/2023

Unclassified Unlimited Release

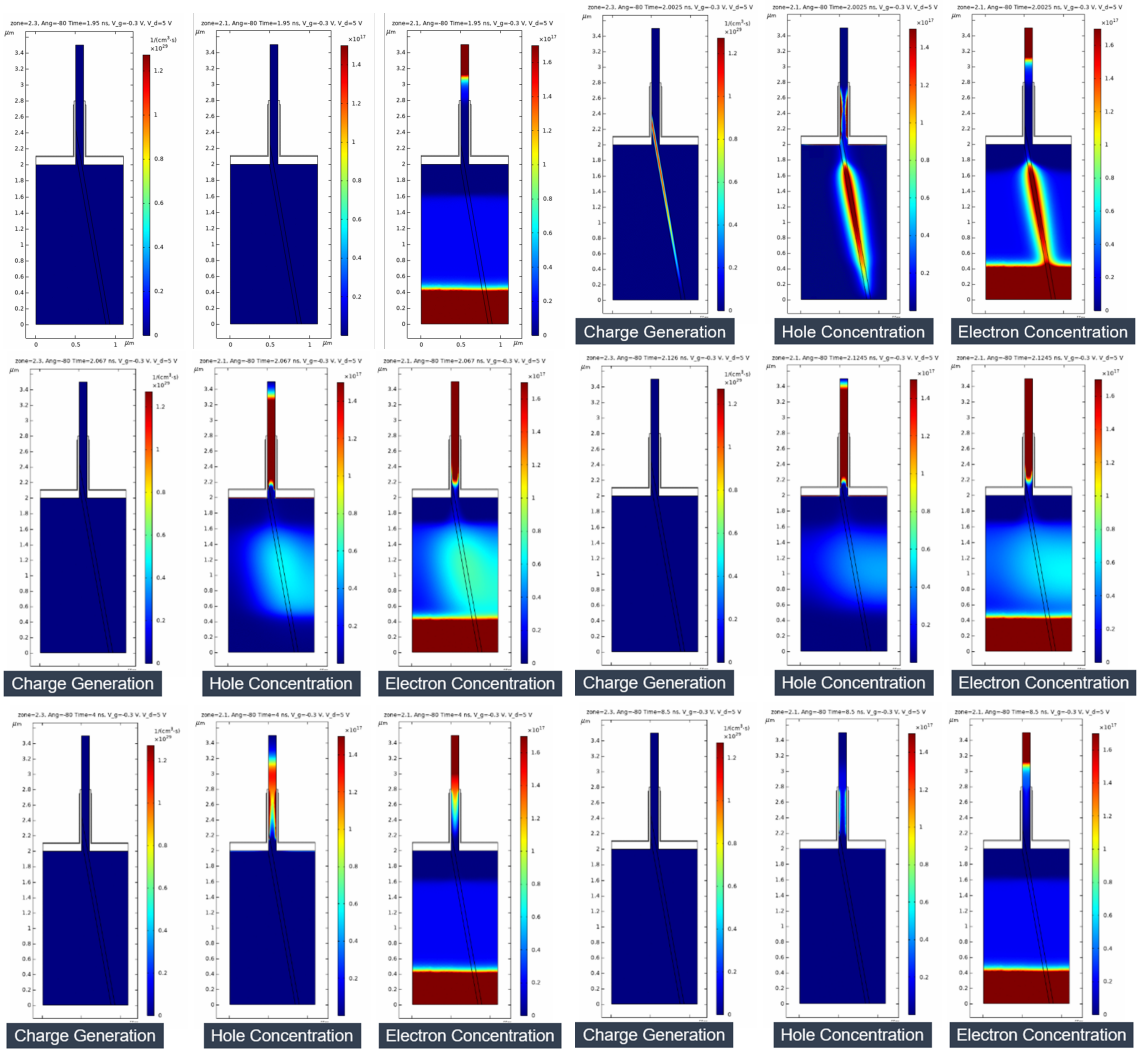

Figure 5.15: *Time-dependent solution snapshots of* 900 keV *alpha particle ionization simulated. Snapshot times:* 1.95 ns, 2.0025 ns, 2.067 ns, 2.126 ns, 4 ns, 8.5 ns.

Fig. 5.19. The spectrum contribution from the alpha particles is shown in Fig. 5.20, and the lithium ions is shown in Fig. 5.21. Also included in Figs. 5.22 and 5.23 are the contributions from the alpha particles incident on the fin edge and base of trench respectively. The lithium ion contributions from particles on the fin edge and base of the trench are shown in Figs. 5.24 and 5.25 respectively. The value of N in the spectra represent the number of particle instances on the surface of the GaN, where the total number of source thermal neutrons simulated was 5,517,789. Because there were 45,229 thermal neutron histories accounted for in the PTRAC output file, about 0.8% of the source thermal neutrons lead to

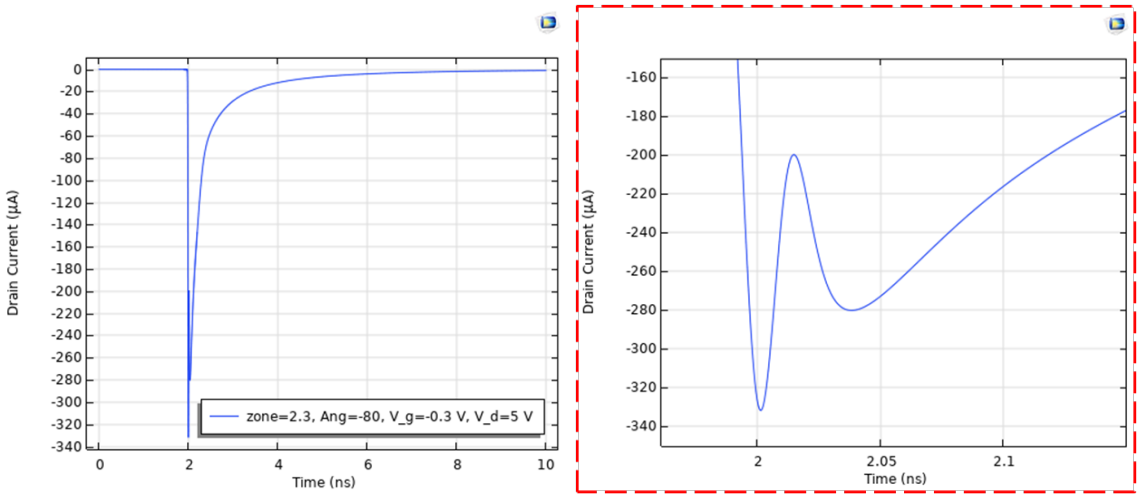

Figure 5.16: *Output drain current from simulated* 900 keV *alpha particle ionization, see Fig. 5.15, full pulse (left) and zoomed in of peak (red outline).*

a reaction product reaching the GaN.

The total integrated charge spectrum shows three main sections, low charge, medium charge, and high charge. The low charge region covers from 0 C to about 0.4×10^{-13} C, the medium charge region covers about 0.4×10^{-13} C to about 0.75×10^{-13} C, and the high charge region cover charge values greater than about 0.75×10^{-13} C.

The low charge region is dominated by alpha particle counts, where nearly all counts greater than 0.15×10^{-13} C are from the alpha particle spectrum. The alpha particles interacting in the fin are most abundant and account for most of the counts in this region. The lithium ions also contribute to the low charge region, but remain almost exclusively below the 0.15×10^{-13} C value. The medium charge region contains scattered counts from 0.4×10^{-13} C to about 0.6×10^{-13} C exclusively from the alpha particle spectrum, mostly from the the fin interactions. More counts begin to accumulate from 0.6×10^{-13} C to about 0.7×10^{-13} C due to the alpha particles reaching the trench at angles near $-120°$. The high charge region is nearly all from the alpha particles entering the trench at or near perpendicular angles (around $-90°$). The maximum charge value in the total spectrum is 1.3×10^{-13} C, most likely from an alpha particle that reached the base of the trench at an angle around $-90°$ and $-60°$.

NSC-614-5769 11/2023
Unclassified Unlimited Release

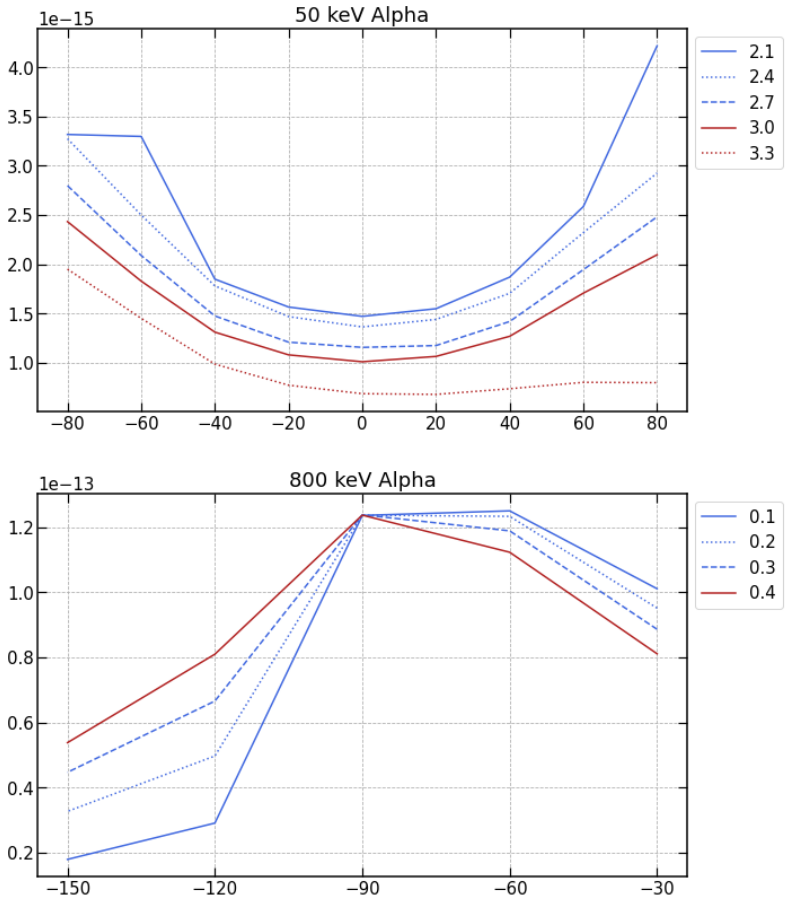

Figure 5.17: *Angular interpolated integrated charge values for* 50 keV *and* 800 keV *alpha particle COMSOL simulations.*

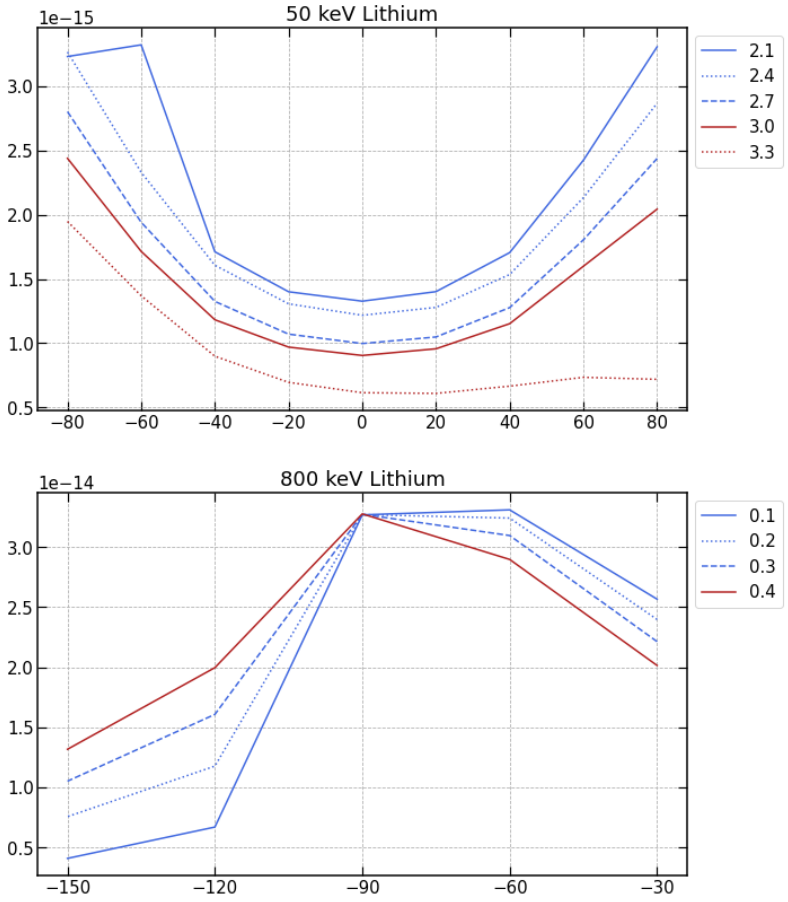

Figure 5.18: *Angular interpolated integrated charge values for* 50 keV *and* 800 keV *lithium ion COMSOL simulations.*

NSC-614-5769 11/2023

Unclassified Unlimited Release

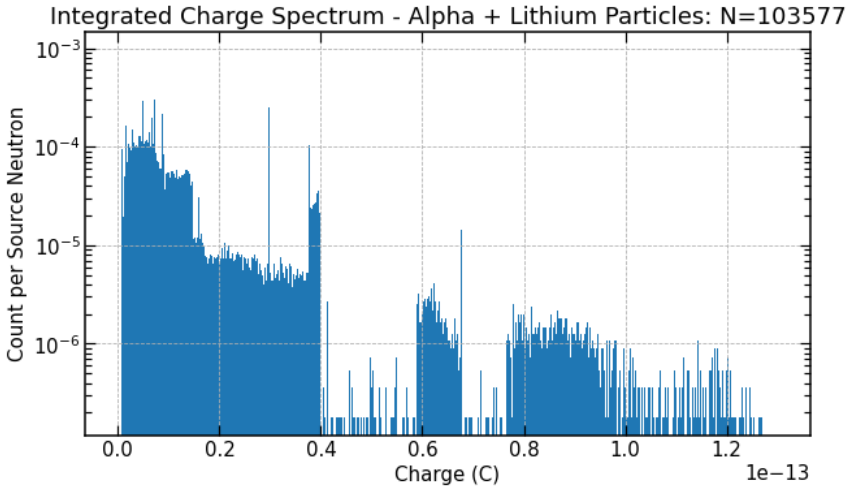

Figure 5.19: *Integrated charge spectrum including alpha particles and lithium ions. The value of N represents the number of times the particles were incident on the GaN surface– the total number of source thermal neutrons simulated was 5,517,789.*

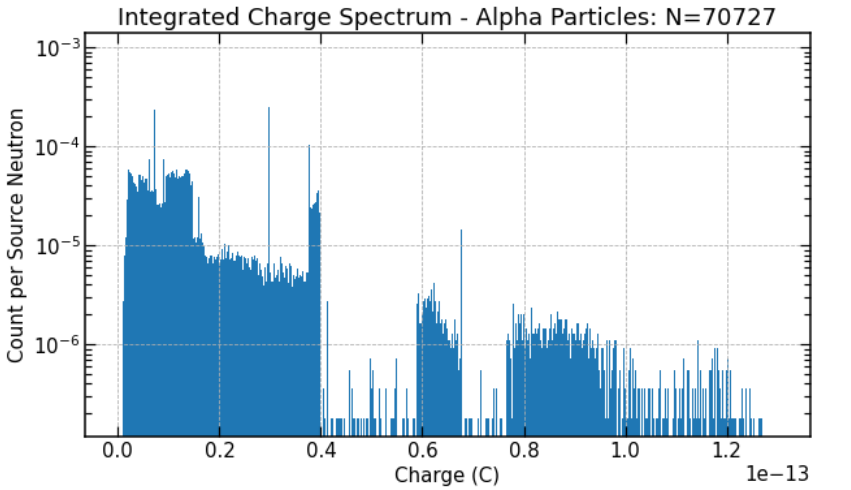

Figure 5.20: *Integrated charge spectrum including only alpha particles. The value of N represents the number of times the particles were incident on the GaN surface– the total number of source thermal neutrons simulated was 5,517,789.*

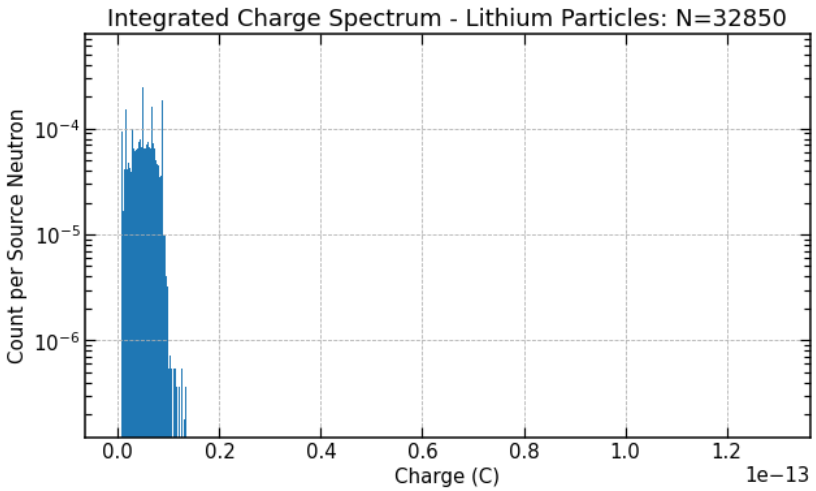

Figure 5.21: *Integrated charge spectrum including only lithium ions. The value of N represents the number of times the particles were incident on the GaN surface– the total number of source thermal neutrons simulated was 5,517,789.*

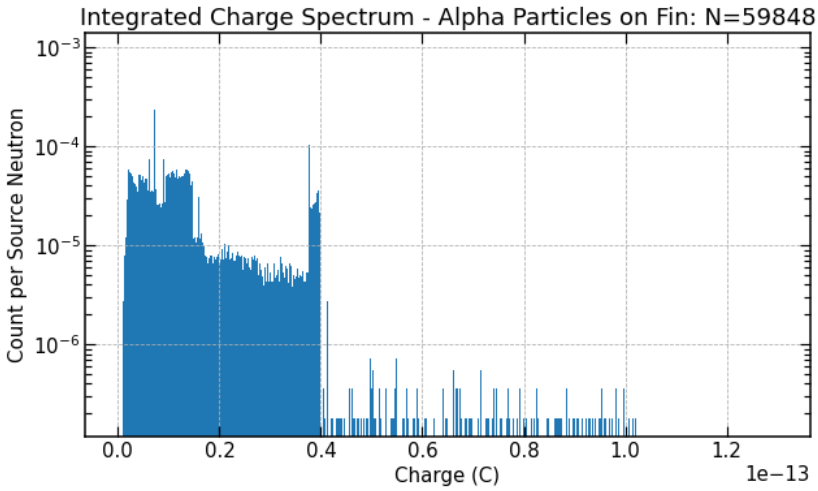

Figure 5.22: *Integrated charge spectrum including only alpha particles incident on fin edge. The value of N represents the number of times the particles were incident on the GaN surface– the total number of source thermal neutrons simulated was 5,517,789.*

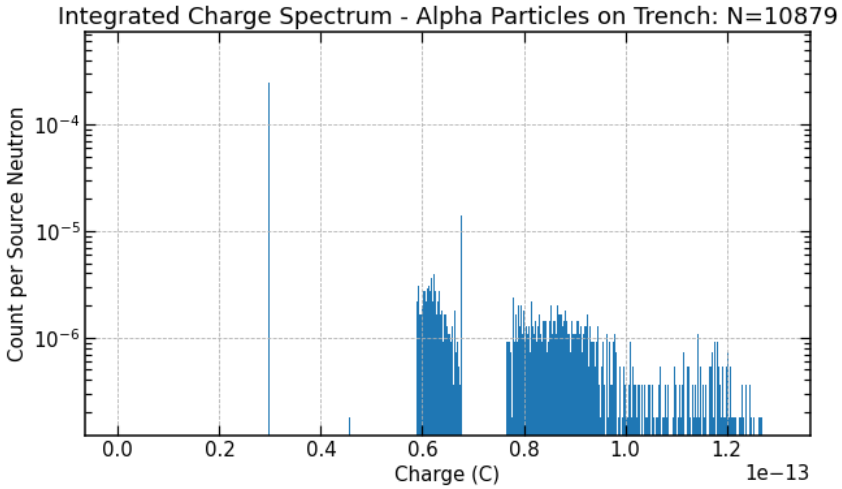

Figure 5.23: *Integrated charge spectrum including only alpha particles incident on base of trench. The value of N represents the number of times the particles were incident on the GaN surface– the total number of source thermal neutrons simulated was 5,517,789.*

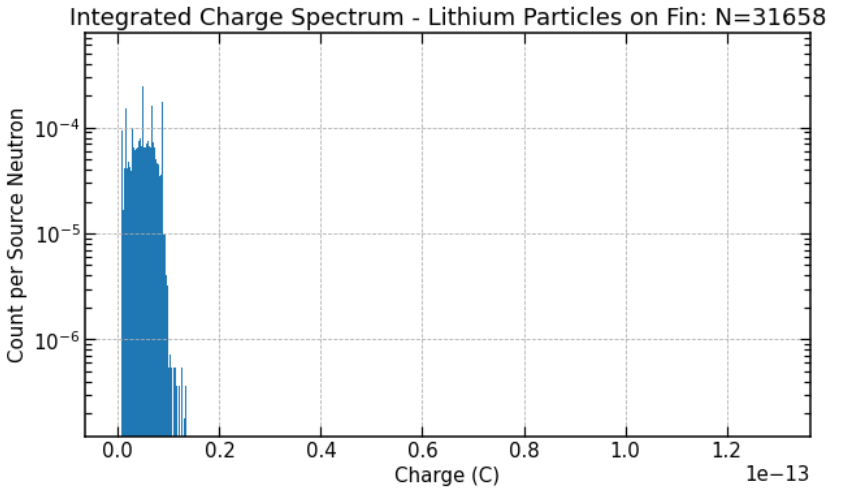

Figure 5.24: *Integrated charge spectrum including only lithium ions incident on fin edge. The value of N represents the number of times the particles were incident on the GaN surface– the total number of source thermal neutrons simulated was 5,517,789.*

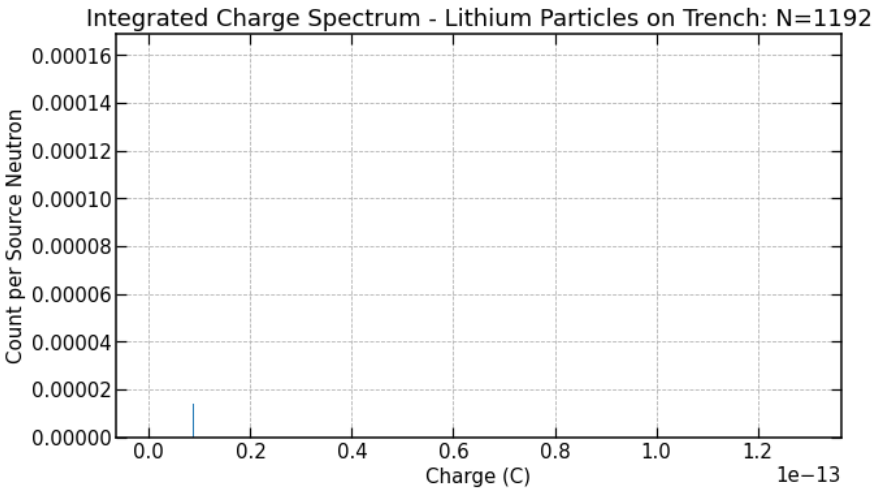

Figure 5.25: *Integrated charge spectrum including only lithium ions incident on base of trench. The value of N represents the number of times the particles were incident on the GaN surface– the total number of source thermal neutrons simulated was 5,517,789.*

NSC-614-5769 11/2023

Unclassified Unlimited Release

Chapter 6

Conclusions

From the radiation transport simulations, it is clear that both of the charged particle from the boron-neutron capture products are capable of reaching the fin, but lithium ions are mostly shielded from reaching the base of the trench of the GaN vertical FinFET. The region near the top of the fin is the most common interaction location. About 15% of the total alpha particle instances reached the trench and around 3% of the lithium ion instances made it to the base of the trench. This implies that most of the radiation-induced damage would be concentrated in the top portion of the device. As for count efficiency, it was found that about 0.8% of the thermal neutrons simulated lead to a reaction product reaching the GaN.

By testing the fabricated GaN vertical FinFETs, it was concluded that the devices were not necessarily consistent in their output current values, on-state resistance, and turn on drain bias. This could be due to multiple factors, including temperature, probe contact, gate leakage current, as well as variation in the FinFETs themselves. The testing of the devices provided insight on the range of output characteristics of real devices, so developing detectors with FinFETs would need to be able to handle the variability, perhaps through operating parameter calibration.

From the stationary electronic transport simulations, it was clear that the device would need to be operated in an off state to minimize background current. By varying the gate bias and drain bias, the operating parameters that maintained an off state and reduced

NSC-614-5769 11/2023

Unclassified Unlimited Release

the counter-pointing electric field lines in the gate region were determined to be $V_S = 0\,V$, $V_G = -0.3\,V$, and $V_D = 5\,V$. By using the results of the fabricated GaN FinFETs, a general tuning of the COMSOL simulation model was made with the GaN material electron mobility adjusted to $200\,cm^2\,V^{-1}\,s^{-1}$. The results of the stationary study show that the sensitive detection region is at the base of the fin due to the large charge separation from the gate to bulk.

From the time-dependent electronic transport simulations, it was shown that the simulated ionization could be detected in an output drain current. A database of output drain current pulses was then collected and converted to induced charge, since the current would most likely be sent to a charge amplifier and convert the charge to an amplified voltage. The difference in electron and hole mobilities lead to holes leaving a longer pulse tail and the electrons, being collected very quickly, to induced a large current value over a short period of time. This meant that much of the integrated charge came from the holes rather than electrons. Through analysis of the electric fields and hole concentration after the ionization, it was clear that holes were being trapped in the region between the gate contacts, and recombination was limited (see Fig 5.15). It is unknown what the effects of multiple ionization events would do in the region between the gates, but it is suspected that the charge separation of the bulk and gate region as well as the top of the fin and the gate region would force an equilibrium and stop allowing holes to build up, but rather recombine.

After combining the radiation transport database with the electronic transport database and creating the integrated charge spectrum from the boron neutron reaction products, the simulated GaN vertical FinFET geometry was shown to be able to detect thermal neutrons. The output charge ranges from near $1 \times 10^{-15}\,C$ to $1.3 \times 10^{-13}\,C$. Most of the counts will come in the region of $0\,C$ to $0.4 \times 10^{-13}\,C$ due to alpha particles and lithium ions ionizing the GaN in the fin. The charge values greater than $0.4 \times 10^{-13}\,C$ come from alpha particles penetrating the base of the trench.

NSC-614-5769 11/2023

Unclassified Unlimited Release

6.1 Future Work

Further tuning of the electronic transport simulations should be implemented in the future to have more accurate simulations. By implementing a custom mobility model, fine tuning of the saturation current values could more closely match a fabricated device[36]. The on-resistance can also be tuned through the junction length of the geometric doping on the drain contact. This action has been shown on the current COMSOL model by adjusting the drift region length with a constant geometric doping junction length, shown in Fig. 6.1.

Work has begun on implementing radiation-induced damage to the COMSOL electronic transport models. This work may be done by means of a custom mobility model that incorporates radiation-induced defects calculated using MCNP radiation transport and a displacement damage response function. This work will rely on accurate tuning and fabricated hardware damage testing in order to see if the simulation framework has predictive capabilities. The idea is that a simulation model, tuned to a fabricated detector, could accurately reproduce a spectrum before and after radiation-induced damage.

Because the sensitive detection region is mostly shielded by the metal gate contacts and dielectric spacers, it would be interesting to see if there would be any sensitivity to scattered gamma rays. The thinking being that high energy gamma rays would lose energy traveling through the pad metals, B_4C, and gate contacts and then be detected in the high sensitivity region. Although GaN does not have much sensitivity to gamma rays due to its low atomic make-up[8], there may be a chance that even a small amount of ionization could be detected if deposited near the base of the fin due to the high electric fields present.

NSC-614-5769 11/2023

Unclassified Unlimited Release

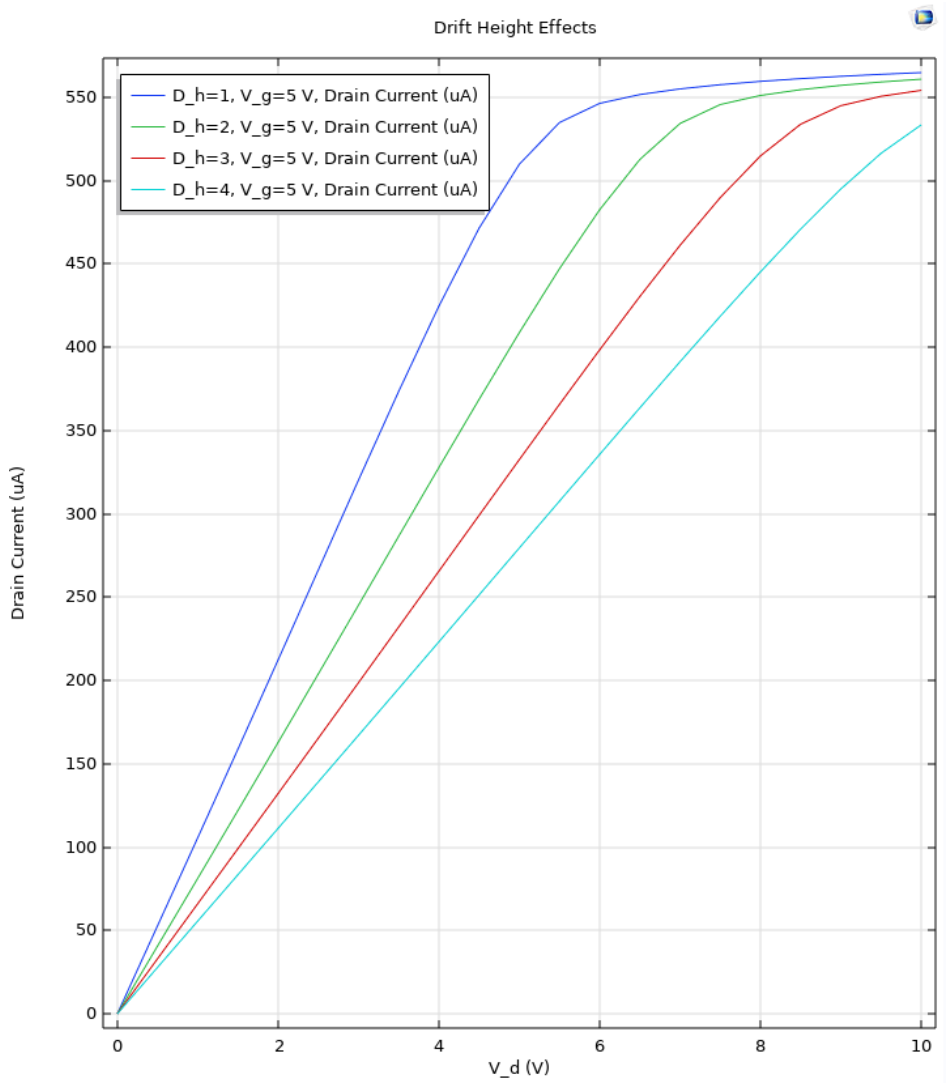

Figure 6.1: *By increasing the drift length (changing how far away the drain contact is to the fin) and maintaining the same geometric doping length in COMSOL, the on-resistance of the GaN FinFET can be tuned.*

NSC-614-5769 11/2023

Unclassified Unlimited Release

Bibliography

[1] H Amano et al. The 2018 gan power electronics roadmap. *J. Phys. D: Appl. Phys.*, 51, 2018.

[2] Kyma Technologies. Low-temperature au-free ohmic contacts to n-gan. *62nd Electronics Material Conference*, 2020.

[3] D. S. McGregor, M. D. Hammig, Y. H. Yang, H. K. Gersch, and R. T. Klann. Design considerations for thin film coated semiconductor thermal neutron detectors - I: Basics regarding alpha particle emitting neutron reactive films. *Nuclear Instruments and Methods in Physics Research, Section A: Accelerators, Spectrometers, Detectors and Associated Equipment*, 500(1-3):272–308, 2003. ISSN 01689002. doi: 10.1016/S0168-9002(02)02078-8.

[4] D. S. McGregor, J. T. Lindsay, and R. W. Olsen. Thermal neutron detection with cadmium1-x zincx telluride semiconductor detectors. *Nuclear Instruments and Methods in Physics Research, Section A: Accelerators, Spectrometers, Detectors and Associated Equipment*, 381(2-3):498–501, 1996.

[5] Albert G. Beyerle and Kenneth L. Hull. Neutron detection with mercuric iodide detectors. *Nuclear Instruments and Methods in Physics Research Section A: Accelerators, Spectrometers, Detectors and Associated Equipment*, 256(2):377–380, 1987. ISSN 0168-9002. doi: https://doi.org/10.1016/0168-9002(87)90236-1. URL https://www.sciencedirect.com/science/article/pii/0168900287902361.

[6] Jinghui Wang, Padhraic Mulligan, Leonard Brillson, and Lei R. Cao. Review of using gallium nitride for ionizing radiation detection. *Applied Physics Reviews*, 2(3), 2015. ISSN 19319401. doi: 10.1063/1.4929913.

NSC-614-5769 11/2023

Unclassified Unlimited Release

[7] John W. Murphy, Lars F. Voss, Clint D. Frye, Qinghui Shao, Kareem Kazkaz, Mark A. Stoyer, Roger A. Henderson, and Rebecca J. Nikolic. Design considerations for three-dimensional betavoltaics. *AIP Advances*, 9(6), 2019. ISSN 21583226. doi: 10.1063/1.5097775. URL http://dx.doi.org/10.1063/1.5097775.

[8] Mutsuhito Sugiura, Maki Kushimoto, Tadashi Mitsunari, Kohei Yamashita, Yoshio Honda, Hiroshi Amano, Yoku Inoue, Hidenori Mimura, Toru Aoki, and Takayuki Nakano. Study of radiation detection properties of GaN pn diode. *Japanese Journal of Applied Physics*, 55(5), 2016. ISSN 13474065. doi: 10.7567/JJAP.55.05FJ02.

[9] Guo Wang, Kai Fu, Chang Sheng Yao, Dan Su, Guo Guang Zhang, Jin Yan Wang, and Min Lu. GaN-based PIN alpha particle detectors. *Nuclear Instruments and Methods in Physics Research, Section A: Accelerators, Spectrometers, Detectors and Associated Equipment*, 663(1):10–13, 2012. ISSN 01689002. doi: 10.1016/j.nima.2011.09.003. URL http://dx.doi.org/10.1016/j.nima.2011.09.003.

[10] Padhraic Mulligan, Jie Qiu, Jinghui Wang, and Lei R. Cao. Study of GaN radiation sensor after in-core neutron irradiation. *IEEE Transactions on Nuclear Science*, 61(4): 2040–2044, 2014. ISSN 00189499. doi: 10.1109/TNS.2014.2320816.

[11] S. F. Mughabghab. Thermal neutron capture cross sections resonance integrals and g-factors, Feb 2003.

[12] C. Zhou, A.G. Melton, and E. et al. Burgett. Neutron detection performance of gallium nitride based semiconductors. *Scientific Reports*, 9(17551), 2019. URL https://doi.org/10.1038/s41598-019-53664-7.

[13] A. Ionascut-Nedelcescu, C. Carlone, A. Houdayer, H.J. von Bardeleben, J.-L. Cantin, and S. Raymond. Radiation hardness of gallium nitride. *IEEE Transactions on Nuclear Science*, 49(6):2733–2738, 2002. doi: 10.1109/TNS.2002.805363.

[14] S.M. Khanna, J. Webb, H. Tang, A.J. Houdayer, and C. Carlone. 2 mev proton radiation damage studies of gallium nitride films through low temperature photoluminescence

NSC-614-5769 11/2023
Unclassified Unlimited Release

spectroscopy measurements. *IEEE Transactions on Nuclear Science*, 47(6):2322–2328, 2000. doi: 10.1109/23.903772.

[15] F. Gaudreau, P. Fournier, C. Carlone, S.M. Khanna, Haipeng Tang, J. Webb, and A. Houdayer. Transport properties of proton-irradiated gallium nitride-based two-dimensional electron-gas system. *IEEE Transactions on Nuclear Science*, 49(6):2702–2707, 2002. doi: 10.1109/TNS.2002.805358.

[16] C. Schwarz, A. Yadav, M. Shatkhin, E. Flitsiyan, L. Chernyak, V. Kasiyan, L. Liu, Y. Y. Xi, F. Ren, S. J. Pearton, C. F. Lo, J. W. Johnson, and E. Danilova. Gamma irradiation impact on electronic carrier transport in AlGaN/GaN high electron mobility transistors. *Applied Physics Letters*, 102(6):062102, 02 2013. ISSN 0003-6951. doi: 10.1063/1.4792240. URL https://doi.org/10.1063/1.4792240.

[17] J. Nord, K. Nordlund, and J. Keinonen. Molecular dynamics study of damage accumulation in gan during ion beam irradiation. *Phys. Rev. B*, 68:184104, Nov 2003. doi: 10.1103/PhysRevB.68.184104. URL https://link.aps.org/doi/10.1103/PhysRevB.68.184104.

[18] V.V. Emtsev, V.Yu. Davydov, V.V. Kozlovskii, G.A. Oganesyan, D.S. Poloskin, A.N. Smirnov, E.A. Tropp, and Yu.G. Morozov. Radiation-produced defects in n-gan. *Physica B: Condensed Matter*, 401-402:315–318, 2007. ISSN 0921-4526. doi: https://doi.org/10.1016/j.physb.2007.08.176. URL https://www.sciencedirect.com/science/article/pii/S0921452607007211.

[19] Douglas S. McGregor, Steven L. Bellinger, and J. Kenneth Shultis. Present status of microstructured semiconductor neutron detectors. *Journal of Crystal Growth*, 379:99–110, 2013. ISSN 0022-0248. doi: https://doi.org/10.1016/j.jcrysgro.2012.10.061. URL https://www.sciencedirect.com/science/article/pii/S0022024812009864. Compound Semiconductors and Scintillators for Radiation Detection Applications: A Special Tribute to the Research of Michael Schieber.

NSC-614-5769 11/2023

Unclassified Unlimited Release

[20] Laramore. D. *Simulation and validation of charge carrier drift in pixelated microstructured semiconductor neutron detectors.* PhD thesis, Kansas State University, 2020.

[21] Sharma. S. *An advanced microstructured semiconductor radiation detector for neutron imaging and oil well logging.* PhD thesis, Kansas State University, 2022.

[22] James Ziegler. JFZ IBM-Web page 001. URL http://www.srim.org/SRIM/SRIMINTRO.htm.

[23] COMSOL Multiphysics® v. 5.6. Semiconductor module. 2021. URL www.comsol.com.

[24] Kyma Technologies. Gan substrates (bulk, c-plane). 2021. URL https://www.kymatech.com/products-services/materials/gan-related-iii-n-materials/490-bulk-gan-c-plane-substrates.

[25] Min Sun, Yuhao Zhang, Xiang Gao, and Tomás Palacios. High-performance gan vertical fin power transistors on bulk gan substrates. *IEEE ELECTRON DEVICE LETTERS*, 38, Apr. 2017.

[26] Min Sun, Yuhao Zhang, Xiang Gao, and Tomás Palacios. Leakage and breakdown mechanisms of gan vertical power finfets. *Appl. Phys. Lett.*, 114, 2019. doi: https://doi.org/10.1063/1.5092433.

[27] Min Sun, Ming Pan, Xiang Gao, and Tomås Palacios. Vertical gan power fet on bulk gan substrate. In *2016 74th Annual Device Research Conference (DRC)*, pages 1–2, 2016. doi: 10.1109/DRC.2016.7548467.

[28] Joshua Perozek, Ayrton Munoz, Tomas Palacios, and United States Massachusetts Institute of Technology Cambridge. Vertical gan fin transistors for power and rf applications. 2019.

[29] Zhongming Zhang and Michael D. Aspinall. Comparison of neutron detection performance of four thin-film semiconductor neutron detectors based on geant4. *Sensors*, 21

NSC-614-5769 11/2023
Unclassified Unlimited Release

(23), 2021. ISSN 1424-8220. doi: 10.3390/s21237930. URL https://www.mdpi.com/1424-8220/21/23/7930.

[30] James W. McCauley. Structure and properties of aluminum nitride and alon ceramics. 2002.

[31] Yuhao Zhang and Tomas Palacios. (ultra) wide-bandgap vertical power finfets. *IEEE Transactions on Electron Devices*, 67(10):3960–3971, 2020.

[32] W. Shockley and W. T. Read. Statistics of the recombinations of holes and electrons. *Phys. Rev.*, 87:835–842, Sep 1952. doi: 10.1103/PhysRev.87.835. URL https://link.aps.org/doi/10.1103/PhysRev.87.835.

[33] Thierry Goudon, Vera Miljanovic, and Christian Schmeiser. On the shockley-read-hall model: Generation-recombination in semiconductors. *SIAM Journal of Applied Mathematics*, 67:1183–1201, 01 2007. doi: 10.1137/060650751.

[34] G. Sabui, P. J. Parbrook, M. Arredondo-Arechavala, and Z. J. Shen. Modeling and simulation of bulk gallium nitride power semiconductor devices. *AIP Advances*, 6(5): 055006, 05 2016. ISSN 2158-3226. doi: 10.1063/1.4948794. URL https://doi.org/10.1063/1.4948794.

[35] Joy Barker and Randy John Shul. High field effects of gan hemts. 9 2004. doi: 10.2172/919143. URL https://www.osti.gov/biblio/919143.

[36] JD Albrecht, RP Wang, PP Ruden, M Farahmand, and KF Brennan. Electron transport characteristics of gan for high temperature device modeling. *Journal of Applied Physics*, 83(9):4777–4781, 1998.

NSC-614-5769 11/2023

Unclassified Unlimited Release